

AUG 7 1958

Copy
RM L58F02

UNCLASSIFIED

C. 1



RESEARCH MEMORANDUM

WIND-TUNNEL INVESTIGATION OF THE LOW-SPEED
STABILITY AND PERFORMANCE CHARACTERISTICS OF A JET-POWERED
LOW-ASPECT-RATIO VERTICAL-TAKE-OFF-AND-LANDING
CONFIGURATION WITH ENGINES BURIED
IN TILTABLE WINGS

By William I. Scallion and Clarence D. Cone, Jr.

Langley Aeronautical Laboratory
Langley Field, Va.

LIBRARY COPY

AUG 7 1958

LANGLEY AERONAUTICAL LABORATORY
LANGLEY FIELD, VIRGINIA

CLASSIFIED DOCUMENT

This material contains information affecting the National Defense of the United States within the meaning of the espionage laws, Title 18, U.S.C., Secs. 793 and 794, the transmission or revelation of which in any manner to an unauthorized person is prohibited by law.

NATIONAL ADVISORY COMMITTEE FOR AERONAUTICS

WASHINGTON

August 6, 1958



NATIONAL ADVISORY COMMITTEE FOR AERONAUTICS

RESEARCH MEMORANDUM

WIND-TUNNEL INVESTIGATION OF THE LOW-SPEED
STABILITY AND PERFORMANCE CHARACTERISTICS OF A JET-POWERED
LOW-ASPECT-RATIO VERTICAL-TAKE-OFF-AND-LANDING
CONFIGURATION WITH ENGINES BURIED
IN TILTABLE WINGS*

By William I. Scallion and Clarence D. Cone, Jr.


SUMMARY

An investigation was made in the Langley full-scale tunnel to determine the low-speed stability and performance characteristics of a model of a jet-powered airplane configuration capable of vertical take-off and landing with engines buried in a tiltable low-aspect-ratio wing. The static longitudinal and lateral characteristics of the configuration were obtained for combinations of angle of attack, wing tilt angles, and thrust coefficients suitable for various take-off and landing flight plans. Several horizontal-tail configurations were studied at three vertical positions. The test Reynolds number and Mach number varied from 1.0×10^6 to 2.7×10^6 and from 0.047 to 0.12, respectively.

The basic data showed that, at zero thrust coefficient and wing incidence (approximately the low-thrust-coefficient level-flight condition), longitudinal stability was obtained only when the span of the horizontal tail was sufficient to have the tips of the tail outboard of the centers of the wing trailing vortices. Increasing the wing incidence caused the model with the high- and mid-position large-span horizontal tails to become longitudinally unstable. At wing incidences above 7.5° , the application of thrust was longitudinally destabilizing. The model was directionally stable for the conditions investigated.

Application of the data to flight-path computations for the airplane showed that vertical take-off transition could be accomplished at a constant thrust and rate of change of wing incidence. Computations made for a level-landing-approach transition indicated that nonlinear variations in wing incidence and thrust as well as additional drag would be required. The longitudinal stability characteristics in the take-off and landing flight transitions were nonlinear for some conditions for the high, mid, and low horizontal-tail configurations.

*Title, Unclassified.



INTRODUCTION

The design of airplanes for efficient cruise operation at Mach numbers of 2.5 and higher leads to the use of very high wing loadings and thrust to weight ratios approaching and exceeding unity. As high wing loadings have led to more critical take-off and landing conditions using conventional means, it is of interest to consider the use of a vertical take-off and landing technique made possible by the high thrust to weight ratios available.

In order to ascertain some of the problems and possibilities of such a system, tests have been conducted in the Langley full-scale tunnel on a model of a high Mach number airplane configuration which would utilize a low-aspect-ratio wing enclosing six engines and mounted to allow wing incidence angles to 90° for vertical take-off and landing. The 3-foot-span model (considered approximately 1/10 scale) was powered by cold jets and was similar to the configurations tested at high Mach numbers. (See refs. 1 and 2.)

The static longitudinal and lateral characteristics of the configuration were obtained for various combinations of angle of attack and wing incidence angle that might be utilized during a transition from vertical to horizontal flight and the effects of thrust and several horizontal tail configurations were evaluated. This report presents the basic data obtained along with an analysis of some possible transition flight paths for an airplane of this type. Also presented for comparison are estimates of conventional take-off and landing distances.

COEFFICIENTS AND SYMBOLS

The positive directions of forces, moments, and angular displacements and the system of axes used are shown in figure 1. Forces were resolved along stability axes and moments were resolved about body axes.

C_L	lift coefficient, $\frac{\text{Lift force}}{q_\infty S}$
C_D'	drag coefficient, $\frac{\text{Longitudinal force}}{q_\infty S}$
C_Y	side force coefficient, $\frac{\text{Side force}}{q_\infty S}$
T'_C	thrust coefficient, $\frac{T}{q_\infty S}$

C_m	pitching-moment coefficient, $\frac{\text{Pitching moment}}{q_\infty S \bar{c}}$ about 0.536 \bar{c}
C_n	yawing-moment coefficient, $\frac{\text{Yawing moment}}{q_\infty S b}$
C_l	rolling-moment coefficient, $\frac{\text{Rolling moment}}{q_\infty S b}$
T	thrust force, lb (acting in plane of wing reference line)
q	dynamic pressure, lb/sq ft
V	velocity, knots
S	wing area, sq ft
c	wing chord, ft
\bar{c}	mean aerodynamic chord, $\frac{2}{S} \int_0^{b/2} c^2 dy$, ft
b	wing span, ft
α	angle of attack of fuselage reference line, deg
i_w	angle of incidence of wing reference line measured from fuselage reference line, deg
i_t	angle of incidence of horizontal tail referenced to fuselage reference line, deg
β	angle of sideslip, deg
δ_i	deflection of intake lip from zero position, deg
δ_j	deflection of tailpipe axis plane from chord plane, deg
C_{Y_β}	rate of change of side-force coefficient with angle of sideslip (slope at $\beta = 0^\circ$), per deg
C_{n_β}	rate of change of yawing-moment coefficient with angle of sideslip (slope at $\beta = 0^\circ$), per deg

C_{l_β} rate of change of rolling-moment coefficient with angle of sideslip (slope at $\beta = 0^\circ$), per deg

ϵ_e effective downwash angle, deg

Subscripts:

w wing

t tail

j jet

i engine intake

∞ free-stream conditions

APPARATUS AND TESTS

Model

The model used in this investigation simulated a vertical take-off aircraft with jet engines buried in a tiltable wing. The wing had an aspect ratio of 0.95 and was located with its axis of rotation passing through the fuselage center line 1.43 \bar{c} from the nose of the model. The wing axis of rotation was located on the jet exit center line 0.54 \bar{c} from the wing leading edge. The wing incidence relative to the fuselage could be varied from 0° to 90° in 7.5° increments. The layout and general dimensions of the model are shown in figure 2 and photographs of the model are shown in figure 3. The fuselage had a fineness ratio of 8.6 (based on maximum diameter) and had no canopy.

The model was provided with five horizontal-tail configurations which could be installed at the three vertical locations designated as high, mid, and low positions in figure 2. Three of the horizontal tails, designated tails 1, 2, and 3 were unswept and had spans of 0.78b, 1.00b, and 1.31b, respectively. The other two tails designated tails 4 and 5 had delta plan forms with tail 4 having a span equal to tail 1 and tail 5 having an area equal to tail 1. All tails were flat plates with shaped leading and trailing edges as shown in figures 2 and 4.

Air System for Thrust Simulation

Thrust conditions scaled to represent the output of six 30,000-pound thrust turbojet engines with afterburning were simulated by

ejecting compressed air from six exhaust jets, three located in each wing panel. Cross-sectional views of the right wing panel are shown in figure 5. The interior of each wing panel was constructed so as to approximate inlet and exit characteristics of jet engines buried in the wing. The wing interior was designed to act as an ejector pump, the primary air flow inducing a secondary airflow through the wing inlet (fig. 5) and thereby insuring appropriate simulation of the wing-inlet flow effects on the overall wing aerodynamics. As shown in figure 5, the entire tailpipe section, including the mixing tubes, could be deflected downward $7\frac{10}{2}^\circ$ by inserting a wedge between the plenum and the primary exhaust tubes to simulate jet deflection.

The primary air was obtained from an external compressor, brought on board through the hollow model support strut, and distributed to the two wing plenum chambers through a Y-branched duct. Labyrinth seals were provided at the junctions of the Y-ducts and wing plenum chambers to isolate the model from the primary air ducting. Each wing panel was tiltable at the labyrinth seal; thus, the wing incidence could be varied.

Thrust was set by throttling the primary air to the necessary plenum pressure as determined from static calibration tests. The calibrations consisted of measuring the thrust developed for various plenum total pressures at zero tunnel velocity at several inlet flow conditions controlled by setting the inlet lip deflection. Plenum total pressures were measured with total-pressure tubes located at the entrance of the primary exhaust tubes. Calibration curves so obtained were used to set the desired thrust during tests.

Tests

Preliminary tests were made to determine the characteristics of the basic model without the horizontal tails at wing incidence angles of 0° , 7.5° , 15° , 30° , and 45° for an angle-of-attack range of -18° to 18° .

The main objective of the test program was to determine the longitudinal characteristics of the model at thrust coefficients and wing-incidence angles considered pertinent to transitional flight; however, tests were first made to determine a horizontal-tail configuration that yielded reasonable longitudinal stability for the level-flight configuration ($i_w = 0^\circ$). These tests were conducted at zero thrust coefficient (approximating the low-thrust-coefficient level-flight condition) through the angle-of-attack range with tails 1 and 3 in the high, mid, and low positions and tails 4 and 5 in the high position. (See fig. 2.) The

effects of wing incidence on the longitudinal characteristics of the model at zero thrust were obtained with tails 1, 3, 4, and 5 in the high position and with tail 3 in the mid and low positions. The data obtained with tail 3 was used to determine the range of thrust values to be used in subsequent tests with thrust applied. All the longitudinal tests with thrust applied were made for wing incidences of 0° , 7.5° , 15° , and 30° with tail 3 in the high, mid, and low positions for thrust-coefficient values that corresponded to those calculated for transitional flight. The effects of jet deflection on the longitudinal characteristics of the model were determined with tail 3 in the mid and low positions. Some tests were made at sideslip angles of -4.85° and -10° and 0° and 15° wing incidence with tail 3 in all three positions.

Forces and moments acting on the model were measured with an internally mounted six-component strain-gage balance. The tests Reynolds number and Mach number varied from 1.0×10^6 to 2.7×10^6 and from 0.047 to 0.12, respectively. Calculations were made for jet-boundary (reference 3) and buoyancy corrections; however, they were small, and therefore were not applied.

RESULTS AND DISCUSSION

Longitudinal Characteristics

Effect of tail configuration.- The results of tests made to find a tail configuration producing static longitudinal stability for the model in the normal flight configuration ($i_w = 0^\circ$) are shown in figures 6 to 13. Initial studies, starting with the basic fuselage (fig. 6) and including the short-span unswept tail (tail 1) mounted at three different vertical positions (fig. 7), showed that this tail did not produce stability for any position tested. It was determined from flow studies that the failure of the tail to produce stability was the result of the very strong wing-tip vortices from the low-aspect-ratio wing which immersed the unswept tail in an unfavorable downwash. (See ref. 4.) In an attempt to alleviate this instability, two tails having their area concentrated further inboard (tails 4 and 5) were briefly tested. These results (fig. 8) failed to show any improvement. The visual observations made in conjunction with these tests, utilizing a yarn streamer to locate the wing trailing vortex field, showed that the vortex at moderate lift coefficients was centered spanwise near the tip of the short-span tails; thus, the complete region from the tips to the fuselage was subjected to increased downwash. A qualitative indication of the path of the vortex in relation to the tail plane is illustrated in figure 9. Because the short-span tails were found to be immersed in an unfavorable downwash field at some airplane attitude regardless of vertical position of

the tail, additional tests were made with tails of increased span (tails 2 and 3) in an attempt to reduce the adverse downwash effects by placing a portion of the tail in the upwash region of the tip vortex. The results of these tests are summarized in figures 10 and 11 and show that it was necessary to use the largest span tail (1.31b) to produce stability through most of the angle-of-attack range. (See fig. 10.) With this configuration, the middle- and low-position tails gave the more nearly linear stability characteristics. (See fig. 11.)

The effects of the wing vortex on the stability contribution of four of the tail configurations tested are presented in figure 12 in the form of effective downwash angle variation with angle of attack computed from the force test results. It is apparent that the only tail configuration not showing a large unfavorable effective downwash variation at positive angles of attack was the large-span tail (tail 3). On the basis of these results the remainder of the test program was conducted with the large-span tail. Some limited tail-effectiveness data for this tail for use in the analysis of its trim capabilities are presented in figure 13. It can be noted from the figure that at a tail incidence of zero the model was stable; however, at tail incidences of 10° , 20° , and -20° longitudinal instabilities were encountered and it might be difficult to attain satisfactory longitudinal stability at trim.

Wing incidence and thrust.- The effects of wing incidence and thrust on the longitudinal characteristics of the model with tail 3 in the high, mid, and low positions are shown in figures 14 to 19. For a given lift coefficient an increase in wing incidence produced a positive increase in C_m . (See figs. 14(b) to 14(d).) This condition resulted from a combination of increased downwash at the tail, increased angle of attack of the tail relative to the downwash, and changes in the dynamic pressure at the tail. The principal effect of wing incidence on the longitudinal stability was to introduce pitch-up instabilities at high positive lift coefficients for the high- and mid-tail configurations. (See fig. 15.) It can be seen from figure 15 that the unstable pitch tendency occurs for the high-tail configuration at zero wing incidence, and the same trend is evident for the mid-tail configuration except that it does not occur until the wing incidence is 7.5° . The longitudinal instability for the high- and mid-tail configurations apparently occurred when the tail surfaces moved into the stronger regions of the downwash field. At 7.5° incidence, the mid-position tail had approximately the same location relative to the wing reference line as did the high-position tail at zero wing incidence.

The effects of thrust on the longitudinal stability of the model are summarized in figure 19. The values of T'_c chosen for these figures were approximately those required for points in the vertical take-off

transition. At low wing incidence thrust had little effect on the longitudinal stability of the model with the high and mid position horizontal tails (figures 19(a) and 19(b)). Thrust effects on C_m were more noticeable at low incidences for the low-horizontal-tail configuration (fig. 19(c)) which was in the immediate downwash region affected by the exhaust of the jets.

At the higher wing incidences (15° and 30°), the addition of thrust was somewhat destabilizing for all three tail configurations and caused the low-tail configuration to be unstable for the thrust coefficient shown. In general, no one tail plan form or vertical location was able to provide acceptable stability for the wing-incidence and thrust-coefficient ranges tested.

Static Lateral Directional Characteristics

The static lateral directional characteristics of the model, with the body alone, the body and the wing, and the body-wing with the vertical tail are shown on figure 20. The lateral directional characteristics of the model with the large horizontal tail for a limited wing incidence and thrust coefficient range are presented in figure 21. The model exhibited no unusual or adverse lateral directional characteristics for the high-, mid-, or low-tail configurations for the conditions shown in figure 21.

The application of thrust at zero wing incidence increased the directional stability (fig. 21(b)) and an increase in wing incidence (fig. 21(c), $T'_c = 0$) and combined wing incidence and thrust (fig. 21(d)) also increased the directional stability. The conditions at positive angles of attack shown in figures 21(c) and 21(d) approximately represent conditions that would be encountered for landing and take-off transitions, respectively.

Application of Data to Take-Off and Landing Characteristics

The following discussion deals with the longitudinal characteristics of a high-speed, jet-powered airplane based on the configuration of this investigation as applied to the vertical transitions as well as to the conventional take-off and landing phases of flight. The airplane was assumed to have a take-off weight of 150,000 pounds and a landing weight of 65,000 pounds and the wing area was assumed to be 960 square feet. These weights were assumed to be the same for both the vertical and conventional take-off and landing configurations; however, it is recognized that different ratios of structural weight to gross weight might exist

for configurations specifically designed for either or both methods of take-off and landing.

The conventional take-off and landing distances over a 50-foot obstacle were estimated for several flight conditions by using modifications of the method of reference 5. Although it is not expected that an airplane specifically designed for vertical take-off and landing operations would attempt either conventional take-off or landing except under emergency conditions, it is of interest to estimate the performance under conventional operation.

Vertical and conventional take-off and landing flight paths were computed by using the data from the wind-tunnel tests, and all curves are necessarily limited to the angle-of-attack and wing-incidence range for which the data were obtained. Inasmuch as complete longitudinal trim data are lacking, the computations were based on untrimmed drag data; however, the general nature of the characteristics of the configurations are believed to be illustrated adequately.

Vertical take-off transition.- As it was previously assumed that the aircraft was a high-speed configuration, operation at "off design" conditions, especially in the transition range, should be kept to a minimum. Several vertical take-off flight paths could be envisioned for the assumed configuration; however, unpublished calculations showed that the optimum transition would be accomplished as rapidly as possible and with a minimum gain in altitude during the transition. The calculated flight path for the assumed configuration through a transition from vertical to horizontal flight is shown in figure 22. The flight path shown approximates an optimum curve, and any differences between the calculated and an optimum path are introduced by the limited range of the wind-tunnel test data used in the calculations. The curve was obtained by using the full available thrust of the engines with afterburning for the greater part of the transition and by varying the wing incidence at a constant rate of 2° per second. The use of a constant thrust and a constant wing-incidence rate indicated that, aside from the stability and control problems involved, transition from vertical to horizontal flight would be relatively straightforward. The static longitudinal characteristics at various stages of transition (from $i_w = 30^\circ$ to $i_w = 0^\circ$) are shown in figure 22 as plots of the variation of C_m with α for the three large-span horizontal-tail positions investigated. Vertical lines are drawn through these plots to indicate the angle of attack at the corresponding point along the flight path. The first plot shows the longitudinal stability of the aircraft in transition when the wing incidence was 30° , the angle of attack was near zero, and the thrust coefficient was 4.46. As can be seen, the high-tail configuration was stable, the mid-tail configuration was about neutrally stable, and the low-tail configuration was slightly unstable.

As wing incidence and thrust coefficient are reduced with increased forward speed, the high-tail configuration becomes somewhat less stable. The low-tail configuration, however, becomes stable at wing incidences below 14° . The stability of the mid-tail configuration varied inconsistently with wing incidence and thrust coefficient. On the basis of the vertical take-off characteristics shown in figure 22, the high-tail configuration appears to offer the best longitudinal stability characteristics in the take-off transition flight range.

With regard to an estimate of the control capabilities of the tail configuration of interest, it is evident (fig. 22) that, for the high incidence cases, the untrimmed pitching-moment coefficients were very large, and at $i_w = 30^\circ$ the values ranged from 0.39 for the high-tail configuration to 0.46 for the mid- and low-tail configurations. Although extensive tail effectiveness data to ascertain the ability of the tail to provide trim are not available, an estimate may be made from the limited data in figure 13. The ΔC_m available for trim was determined from the following relationships:

$$(\Delta C_m)_{\text{available for trim}} = (\Delta C_m)_{\text{maximum tail}} - (\Delta C_m)_{\text{downwash}}$$

where

$$(\Delta C_m)_{\text{maximum tail}} = (C_m)_{\text{tail on; maximum tail lift; } \alpha = 0^\circ} - (C_m)_{\text{tail off; } \alpha = 0^\circ}$$

and

$$(\Delta C_m)_{\text{downwash}} = (C_m)_{\text{tail on; } i_t = 0^\circ} - (C_m)_{\text{tail off}}$$

As an example, the effectiveness data for the mid-tail configuration are shown in figure 13 and from this figure the value of ΔC_m (max. tail) at zero angle of attack is shown to be approximately 0.26. It may be assumed that this value is nearly correct for all three configurations (high, mid, or low tail) and for this example, the trim characteristics of the high-tail configuration at $i_w = 30^\circ$, $T'_c = 4.46$, and $\alpha = -0.1^\circ$ as shown on figure 22 will be used. The value of ΔC_m required for trim for this case is -0.39. Referring to figure 19(a) for the $i_w = 30^\circ$, $T'_c = 0$ condition, the value of ΔC_m (downwash) is found to be 0.1. The algebraic sum of ΔC_m (max. tail) as determined previously and ΔC_m (downwash) then is -0.36 and this value is the ΔC_m available for trim. The difference between the ΔC_m required for trim and the ΔC_m available for trim is 0.03. It can be noted in figure 19(a) that an additional increment of ΔC_m (downwash) caused by thrust (the difference between

the curves for $T'_c = 0$ and $T'_c = 4.59$ at $i_w = 30^\circ$) was not included because the portion of the additional C_m that was caused by increased downwash at the tail was not known. It may be reasonably assumed that part of this additional pitching moment was a result of additional downwash at the tail and that trim could be obtained; however, it may be marginal, and, as figure 13 shows, instability may result. Similar analysis when applied to the points along the flight curve corresponding to the lower wing incidences indicates generally that the trim capability became less marginal with decreasing wing incidence and thrust coefficient.

Vertical landing transition.- The transition from high-speed horizontal flight to low-speed vertical descent for landing would appear to be somewhat more complicated than the vertical take-off transition. In vertical take-off, the full thrust of the engines was used; however, in landing, the thrust must be varied, and very careful programming of the changes in thrust in conjunction with simultaneous increases in wing incidence would be required to accomplish transition without an appreciable gain in altitude. Additionally, some method of reducing the forward velocity would be required, such as gaining altitude or, in the case of transition at nearly constant altitude, adding external drag. The calculated flight paths for three types of landing transition are shown in figure 23.

A pull-up maneuver at zero wing incidence in which the forward velocity is reduced by gaining altitude is shown by circle symbols in figure 23(a). Once the velocity is reduced, sufficient thrust would be applied to support the aircraft, the fuselage would be rotated to horizontal, and a vertical descent accomplished. An objectionable feature of this type of transition would be the altitude through which vertical descent utilizing the engine thrust would be made. In this case a vertical descent of approximately 4,700 feet would be required to reach the initial entry altitude.

A modified climbing transition in which the wing incidence was varied at a constant rate of 5° per second is shown by the square symbols in figure 23(a). The altitude gained for this type of transition was 1,200 feet, which is a considerable reduction in altitude over that of the zero-incidence climb transition.

The third type of transition (fig. 23(b)) simulated entry into a nearly constant altitude transition. The slight descent shown by the curve corresponded to a rate of descent of approximately 600 feet per minute. This flight path is more complicated than the two previous ones in that the wing incidence was increased slowly at the beginning of the approach and rapidly near the last calculated point along the curve; therefore, the rate of incidence variation with time was non-linear. The horizontal distance required for this type of transition

was considerably larger than that of the climb transition because it was dependent upon the drag of the configuration rather than upon a gain in altitude to dissipate the forward velocity. Calculations showed that this distance could be reduced by approximately 40 percent by using speed brakes with a drag coefficient of 0.05. At the last calculated point ($i_w = 31^\circ$) thrust was added to maintain altitude and the forward component of thrust was canceled by deploying a drag parachute of approximately 0.155 wing area. The drag coefficient of the parachute based on the data of reference 6 was 0.10. Although this was the last point for which data were available, approximate calculations showed that increases in thrust and wing incidence would occur at a higher rate than during the initial approach.

The small stability plots in figures 23(a) and 23(b) indicate that the configuration with the low tail was longitudinally stable or neutrally stable at all points along the flight paths shown and the mid-tail configuration was unstable at $i_w = 6^\circ$ and 15° . The high-tail configuration was longitudinally stable at the trim angle of attack for most of the conditions shown; however, instabilities were encountered at the higher angles of attack (above approximately 10°) for the vertical climb transition ($i_w = 0^\circ$) and for the modified climb transition at $i_w = 15^\circ$. (See fig. 23(a).) Additionally, the trim angle of attack for the level transition was near the angle of attack for longitudinal instability at $i_w = 15^\circ$. (See fig. 23(b).) The instabilities associated with the high-tail configuration in the landing approach condition are not consistent with the vertical take-off condition, whereas, as previously mentioned, the configuration was longitudinally stable for all conditions shown. (See fig. 22.)

The opposite was found to be true for the low-tail configuration in that the configuration was longitudinally stable for the vertical landing approach and was unstable for some conditions in the vertical take-off transition.

The mid-tail configuration was longitudinally unstable for certain conditions in either the vertical take-off or vertical landing approach phase of flight. The final choice of a horizontal-tail location would depend upon the phase of flight (vertical take-off or landing) for which the longitudinal instabilities associated with the tail locations would be less undesirable and upon the high-speed flight stability conditions (refs. 1 and 2) and structural requirements.

Conventional take-off.- Figure 24 presents the estimated take-off distances for different conditions using conventional take-off procedures. Two take-off conditions were assumed, one with full engine thrust and one with two engines not operating. In each case the take-off velocity was determined by the assumed condition of $\alpha = 12^\circ$ and $i_w = 15^\circ$ at

take-off. Lift was determined by the direct addition of wing-fuselage lift with the lift component of the thrust. It does not include the small induced lift that would be present because of a jet-induced circulation for the aspect-ratio-0.95 wing. The polar of figure 14(d) was used to establish the drag values. No allowance was made for ground effect; thus, the estimated distances should be conservative.

With full thrust, the total take-off distance to clear a 50-foot obstacle is 1,770 feet, of which 1,470 feet is ground distance, 200 feet is transition distance from take-off to climb attitude and 100 feet is the climb distance. The 15° wing incidence was assumed to be held constant during the take-off and climb. The take-off speed was 178 knots.

With two engines inoperative, the take-off distance to clear a 50-foot obstacle was increased to 3,160 feet, of which 2,860 feet was ground distance. The take-off speed was 206 knots. Thus even with two engines not operating the airplane should be able to use existing airfields for take-off, insofar as distance requirements are concerned.

Conventional landing.- The conventional landing characteristics of the configuration are also shown in figure 24. The two landing configurations considered employed 15° and 0° wing incidence at a touchdown angle of attack of 16° . For the 15° incidence case the average lift-drag ratio for the glide region was 1.94. The total landing distance to clear a 50-foot obstacle was 4,930 feet, of which 4,320 feet was ground distance. The touchdown velocity was 146 knots.

The landing distance for the $i_w = 0^\circ$ configuration was 7,022 feet, of which 5,680 feet was ground roll. The touchdown speed was raised to 167 knots by the lower wing incidence.

These results indicate that an aircraft of this type could operate conventionally from existing airfields insofar as distances are concerned.

SUMMARY OF RESULTS

The results of an investigation to determine the low-speed stability and performance characteristics of a model of a jet-powered configuration capable of vertical take-off and landing with engines buried in tiltable wings may be summarized as follows:

1. At zero thrust coefficient and zero wing incidence, longitudinal stability was obtained only when the span of the horizontal tail was sufficient to have the tips of the tail outboard of the center of the trailing vortices of the low-aspect-ratio wing.

2. At increased wing incidence angles, the model with the large-span horizontal tail in the low position was longitudinally stable and the mid- and high-tail configurations were unstable at high angles of attack.

3. The application of thrust at wing incidences above 7.5° was longitudinally destabilizing, and the low-horizontal-tail configuration was unstable at wing incidences of 15° and 30° when thrust was applied.

4. The model exhibited no unusual or adverse lateral directional characteristics for the several conditions investigated that approximated some phases of the transition flight regime.

5. Flight-path computations using the test data indicated that take-off transition was relatively straightforward in that a constant thrust and a constant rate of change of wing incidence could be utilized.

6. Flight-path calculations further indicated that vertical landing transition was somewhat complicated because nonlinear variations in wing incidence and thrust with time and additional drag would be required.

7. In general, no one tail plan form or vertical location was able to provide acceptable stability for the wing-incidence and thrust-coefficient range for both the take-off and landing flight transitions.

Langley Aeronautical Laboratory,
National Advisory Committee for Aeronautics,
Langley Field, Va., May 21, 1958.

REFERENCES

1. Jones, Robert A., and Rainey, Robert W.: Wind-Tunnel Investigation of Two Vertical-Take-Off-and-Landing Jet Bomber Airplanes at Mach Numbers of 1.94 and 2.40. NACA RM L56H22a, 1956.
2. Lord, Douglas R.: Longitudinal Stability Investigation of a Vertical-Take-Off-and-Landing Airplane Configuration With Simulated Jet Intake and Exhaust at Mach Numbers of 1.61 and 2.01. NACA RM L57K05, 1958.
3. Katzoff, S., and Hannah, Margery E.: Calculation of Tunnel-Induced Upwash Velocities for Swept and Yawed Wings. NACA TN 1748, 1948.
4. Jaquet, Byron M.: Some Low-Speed Wind-Tunnel Experiments Pertaining to the Longitudinal Stability Characteristics of a 35° Swept-Wing Model and an Unswept-Wing Model. NACA RM L53H31, 1953.
5. Perkins, Courtland D., and Hage, Robert E.: Airplane Performance - Stability and Control. John Wiley & Sons, Inc., 1953.
6. Scher, Stanley H., and Gale, Lawrence J.: Wind-Tunnel Investigation of the Opening Characteristics, Drag, and Stability of Several Hemispherical Parachutes. NACA TN 1869, 1949.

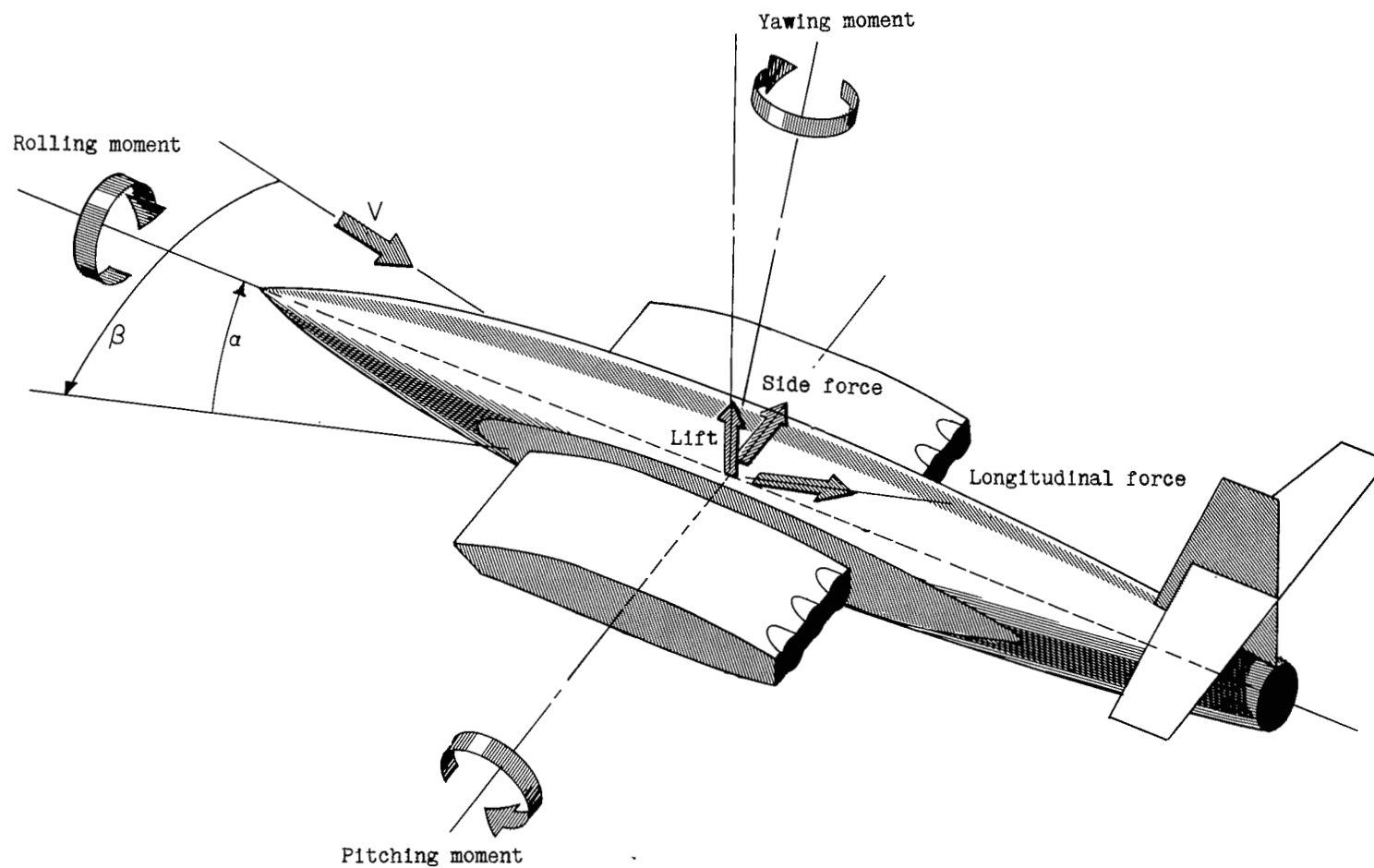


Figure 1.- System of axes used. Positive directions of forces and moments are shown by the arrows.

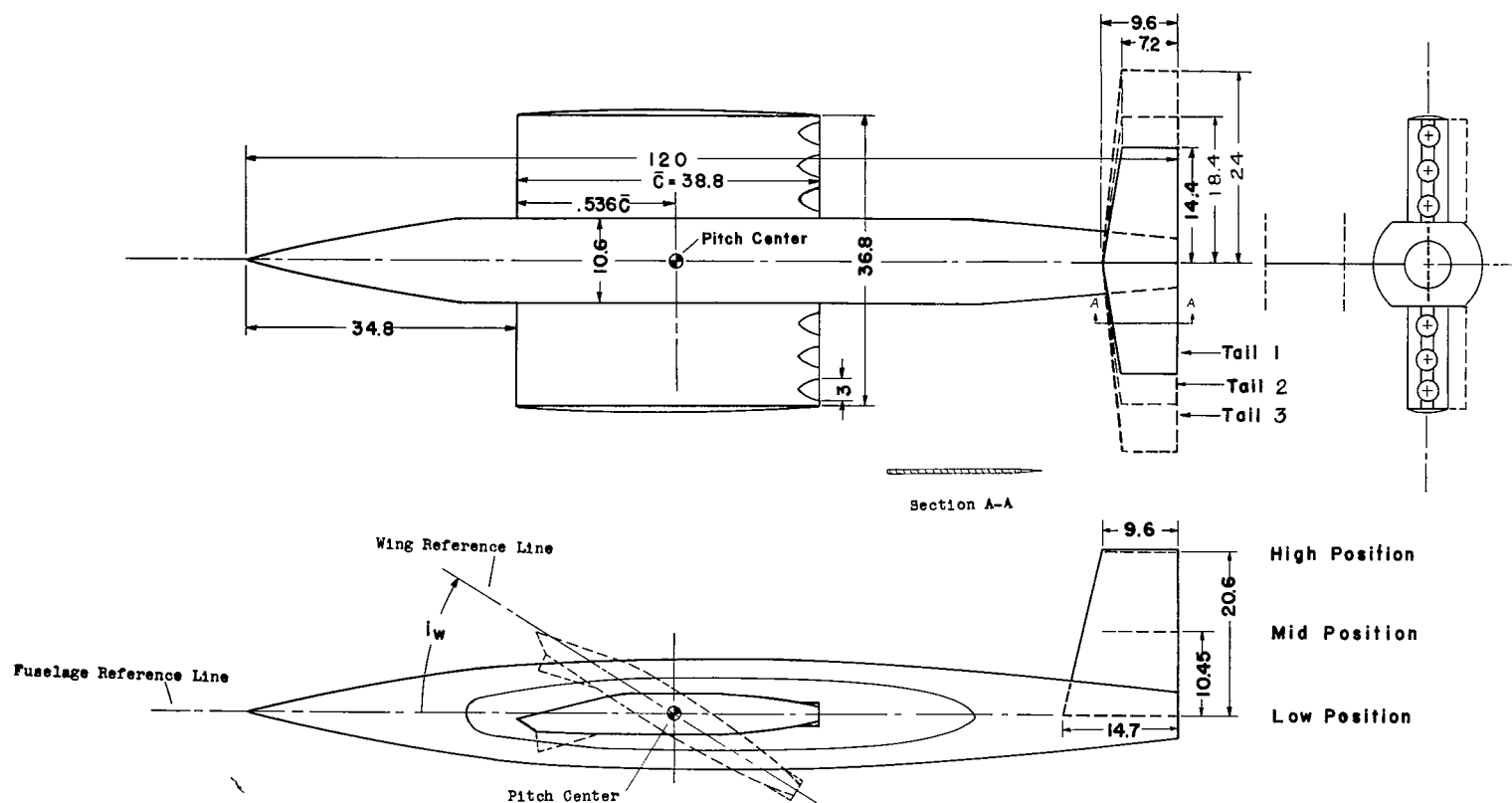
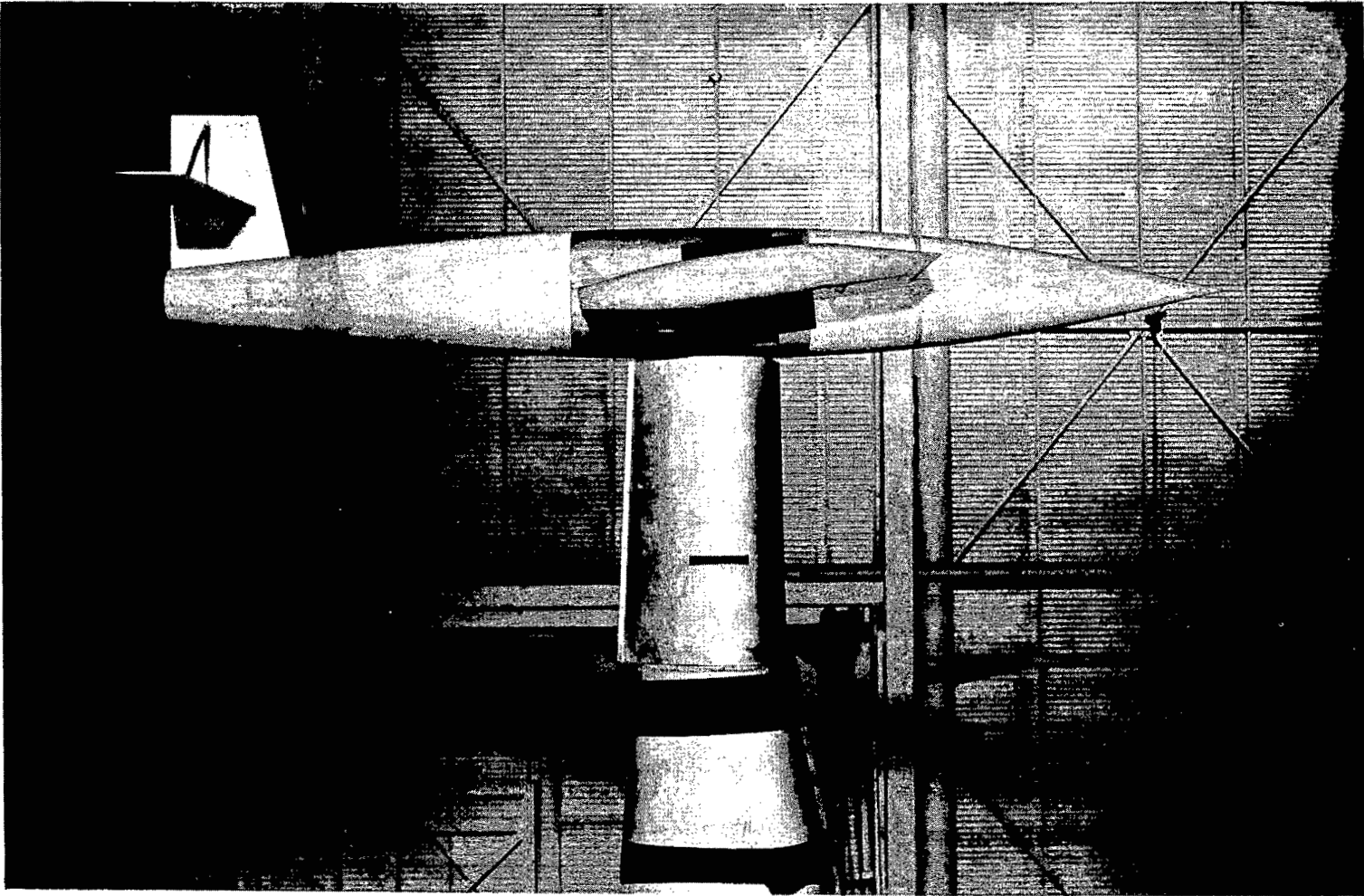
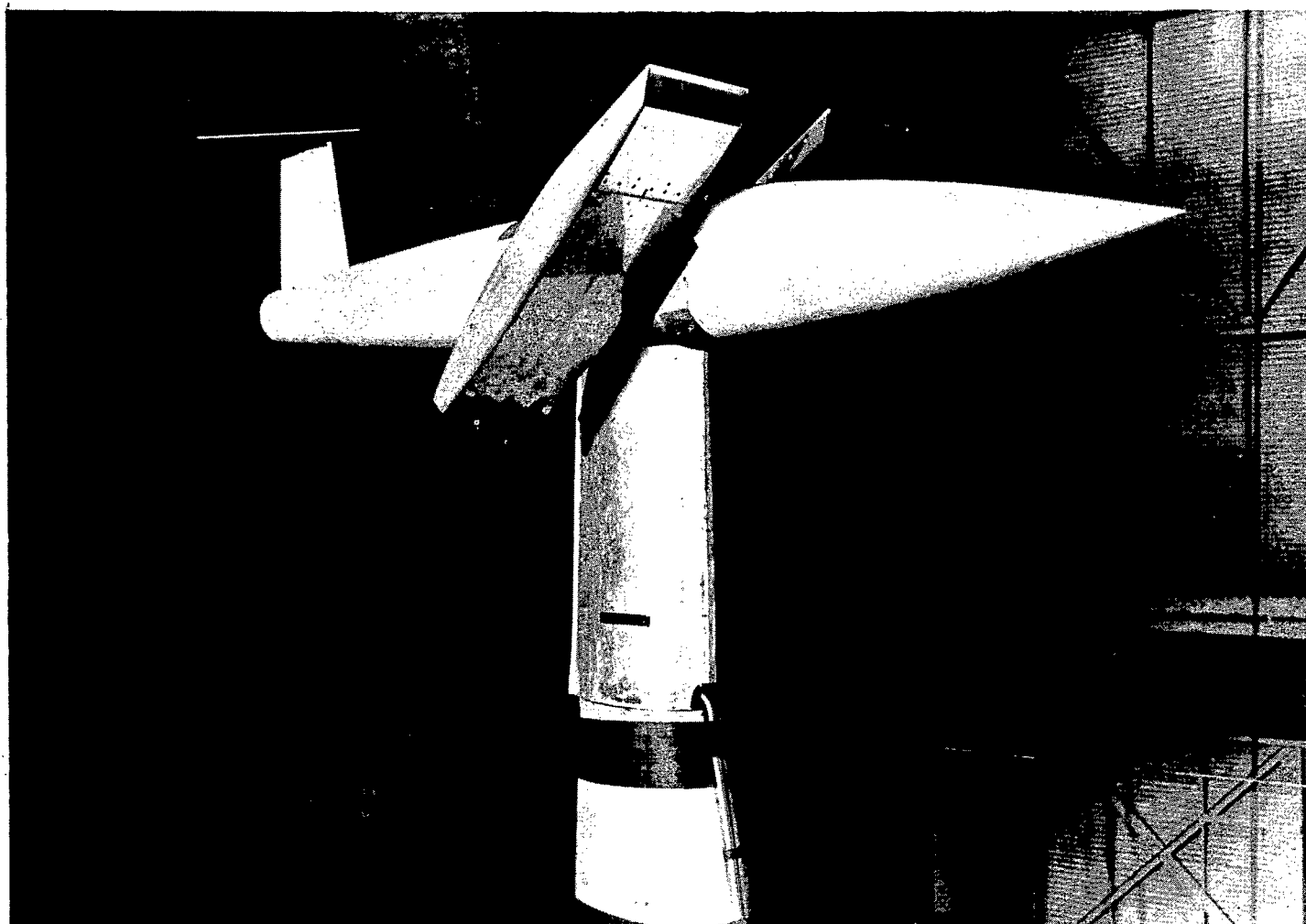


Figure 2.- Three-view sketch of the model. All dimensions are in inches unless otherwise noted.



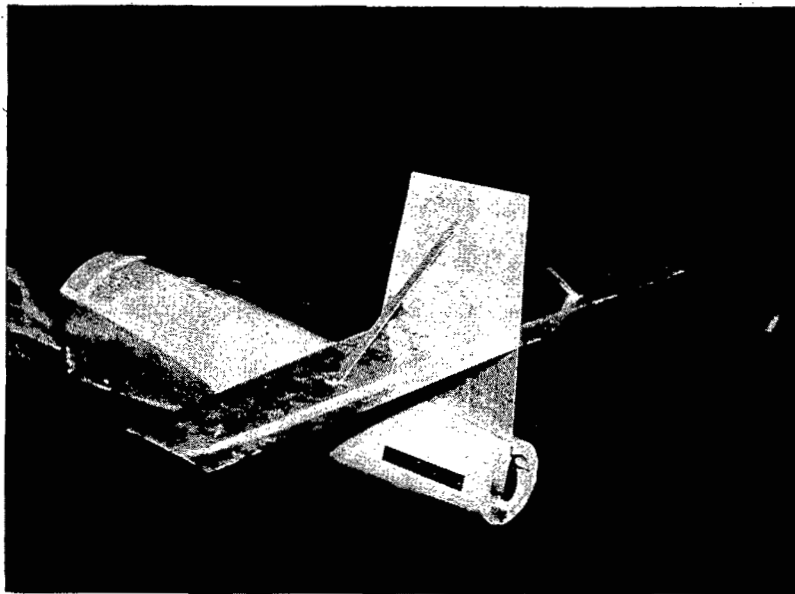
(a) Complete model; $i_w = 7.5^\circ$. L-57-300

Figure 3.- Photographs of the model.



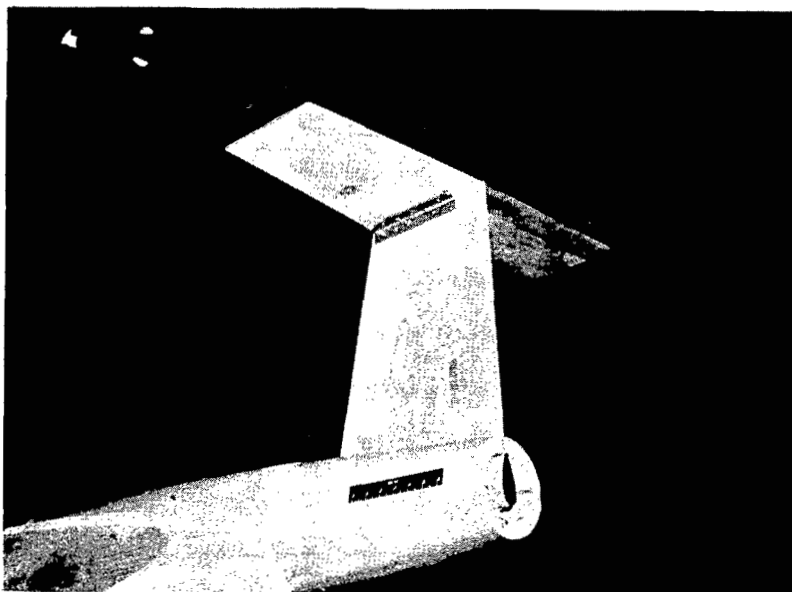
(b) Complete model; $i_w = 45^\circ$. L-57-301

Figure 3.- Continued.



Tail 3, mid position.

L-57-313

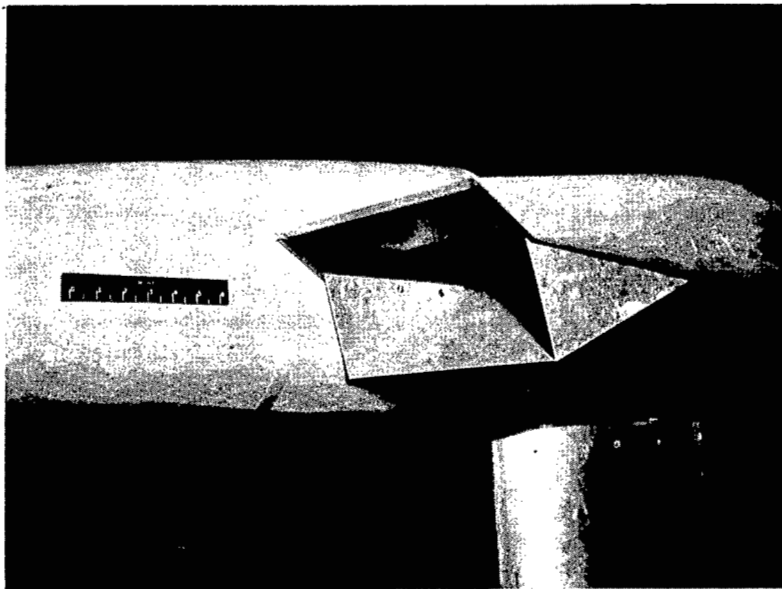


Tail 1, high position.

L-57-312

(c) Details of the horizontal tails.

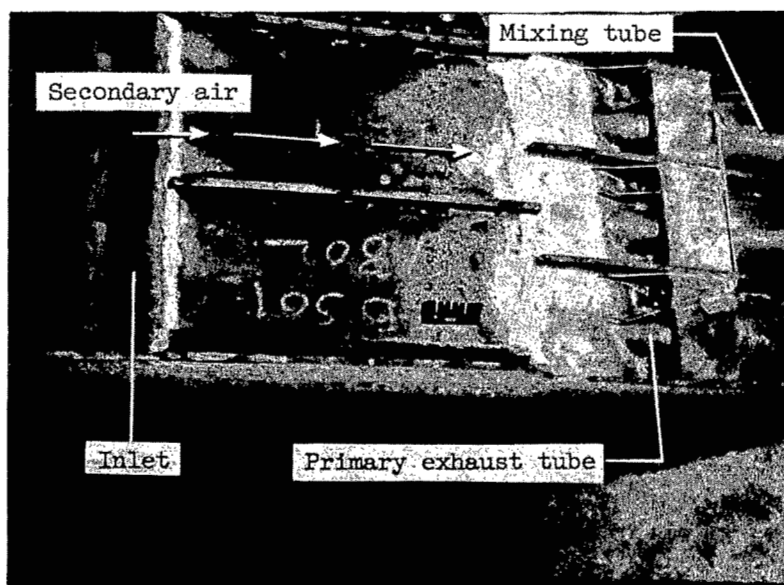
Figure 3.- Continued.



$$\delta_1 = 30^\circ.$$

L-57-306

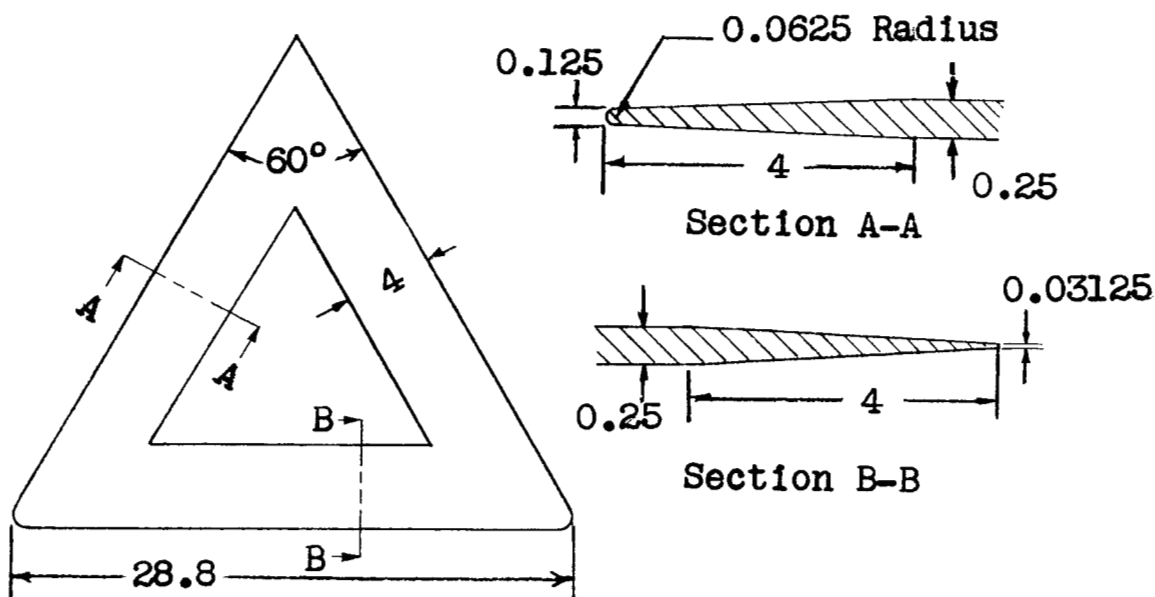
(d) Details of the leading-edge inlets.



(e) Left wing panel, top skin removed. L-57-303.1

Figure 3.- Concluded.

Tail 4



Tail 5

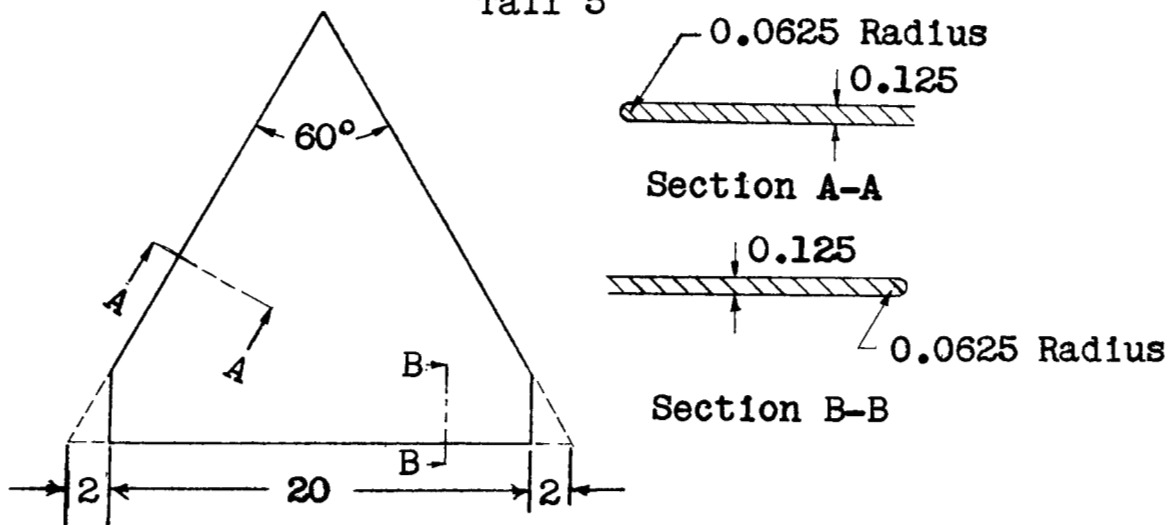


Figure 4.- Plan form and dimensions of tails 4 and 5. All dimensions are in inches unless otherwise noted.

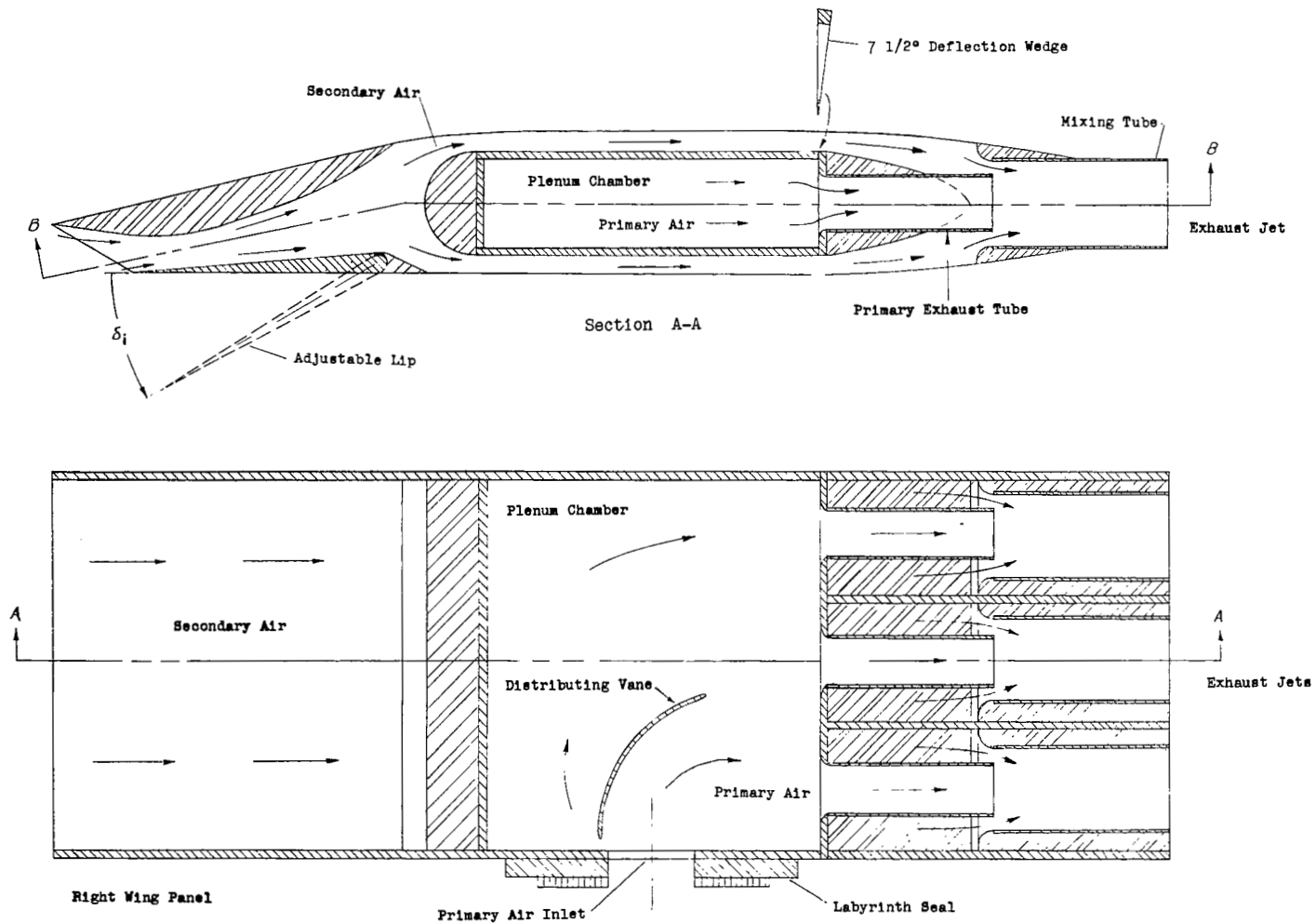


Figure 5.- Details of the wing intake and ejector system.

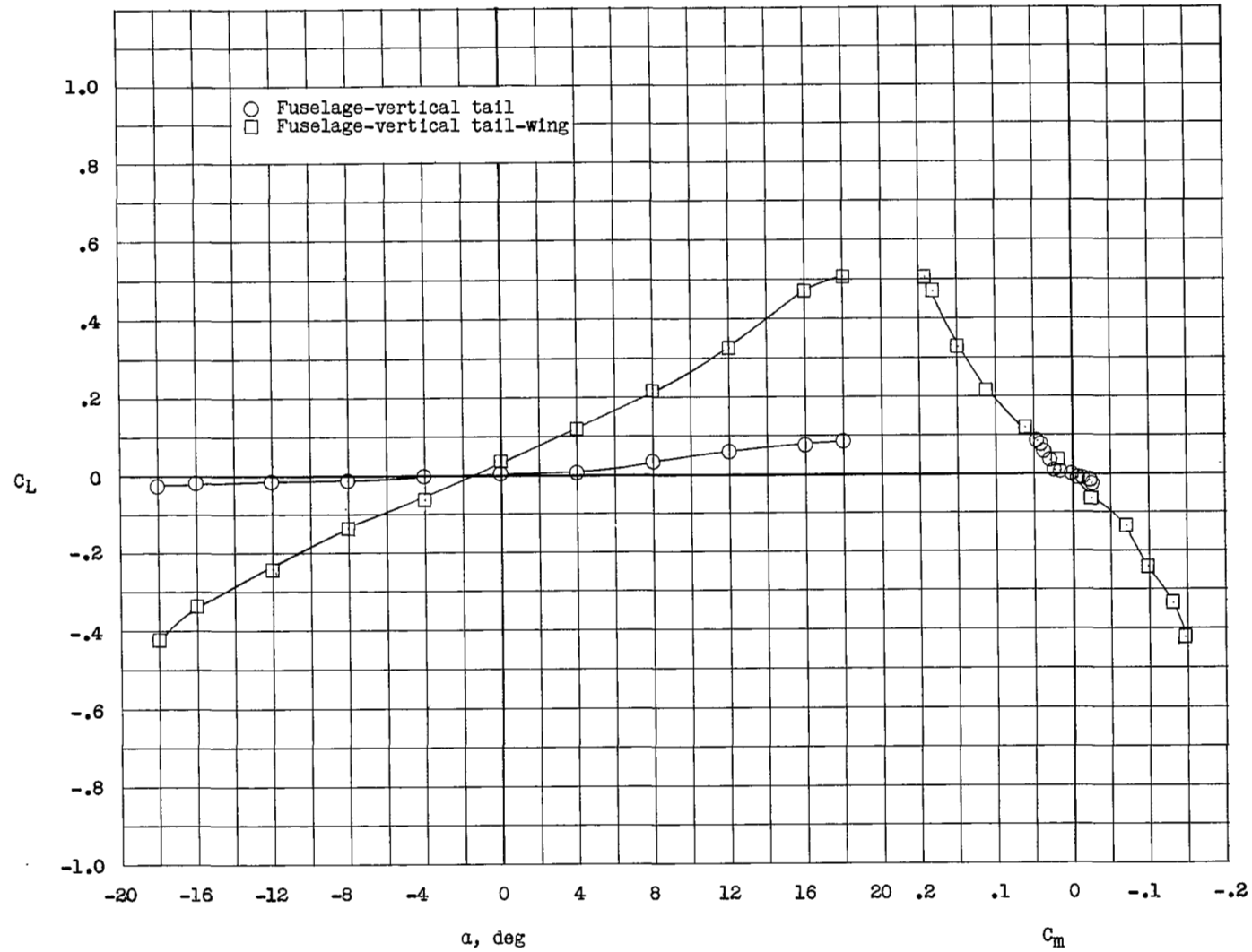


Figure 6.- Longitudinal characteristics of the basic model with the horizontal tail removed.
 $i_w = 0^\circ$; $T'_c = 0$.

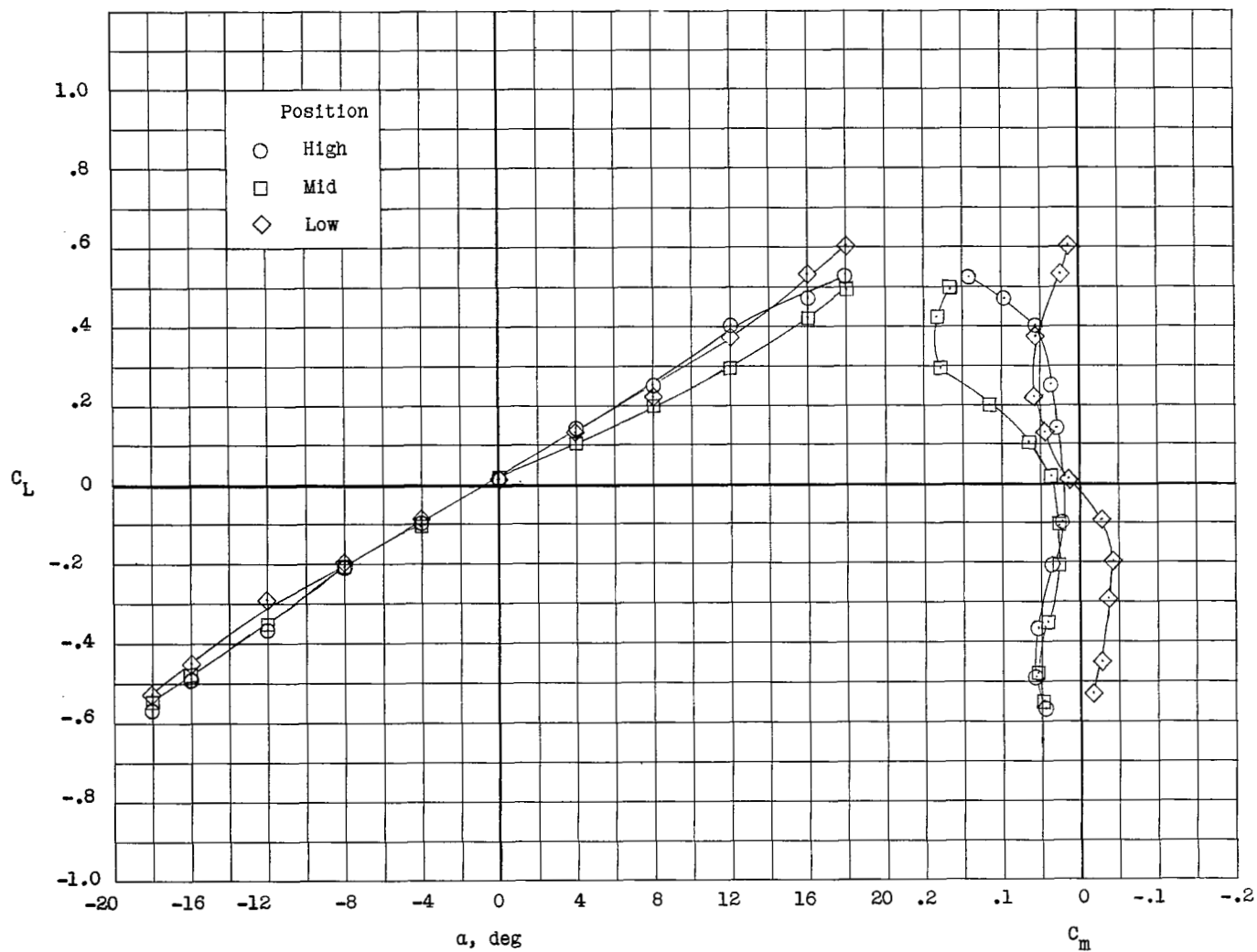


Figure 7.- Longitudinal characteristics of the model with tail 1. $i_w = 0^\circ$; $T'_C = 0$.

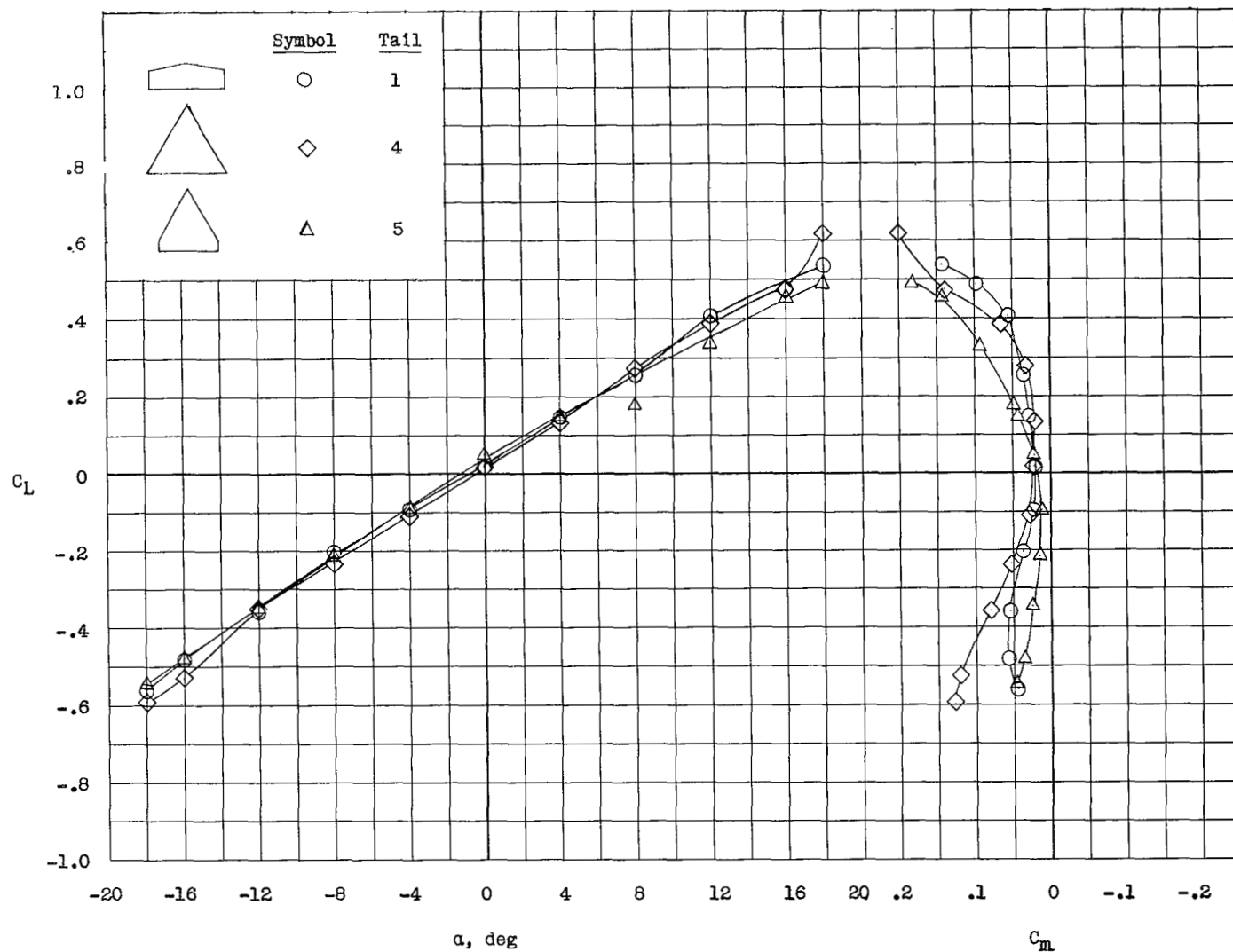


Figure 8.- Effect of plan form on the longitudinal characteristics of the model with the horizontal tail in the high position. $i_w = 0^\circ$; $T'_c = 0$.

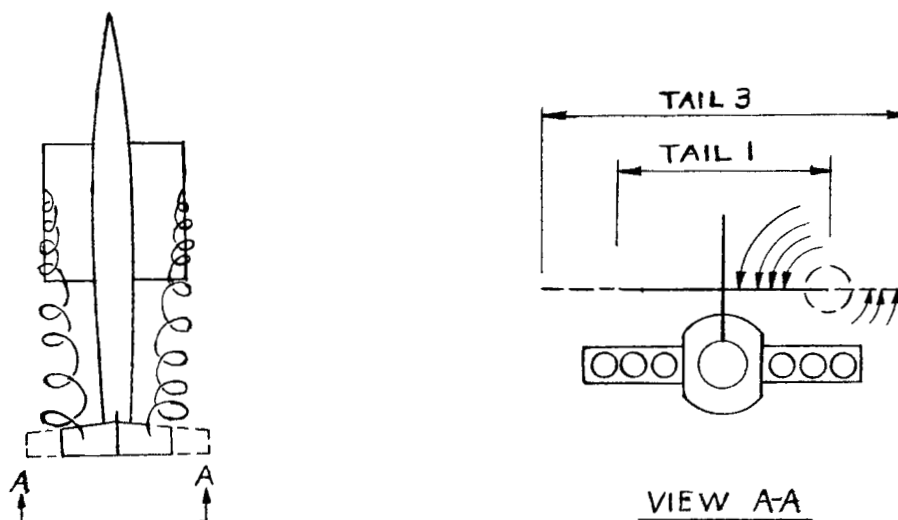


Figure 9.- Illustration of the paths of the tip vortices showing the effect of their downwash on the horizontal tails at angle of attack.

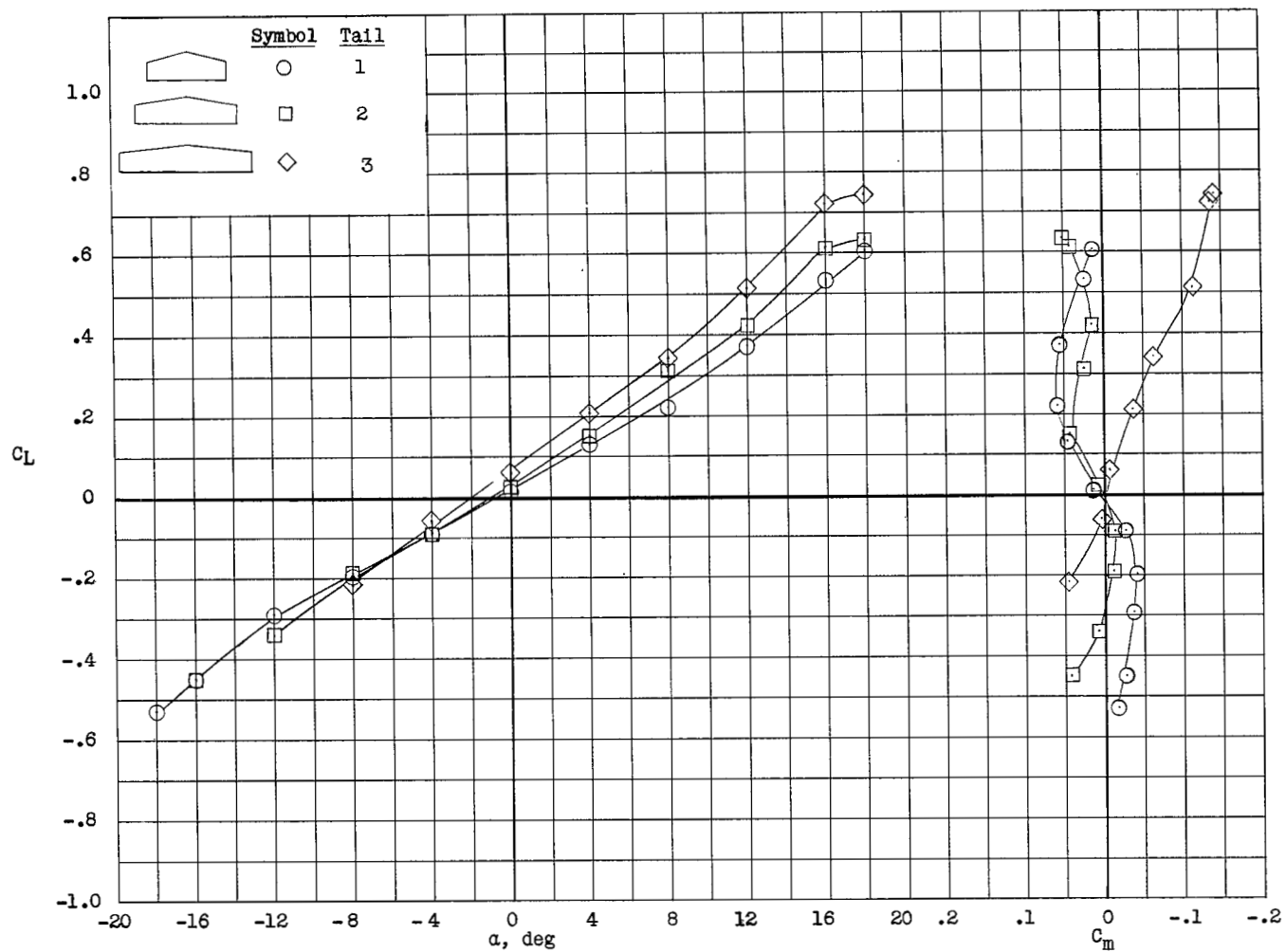


Figure 10.- Effect of tail span on the longitudinal characteristics of the model with the horizontal tail in the low position. $i_w = 0^\circ$; $T'_C = 0$.

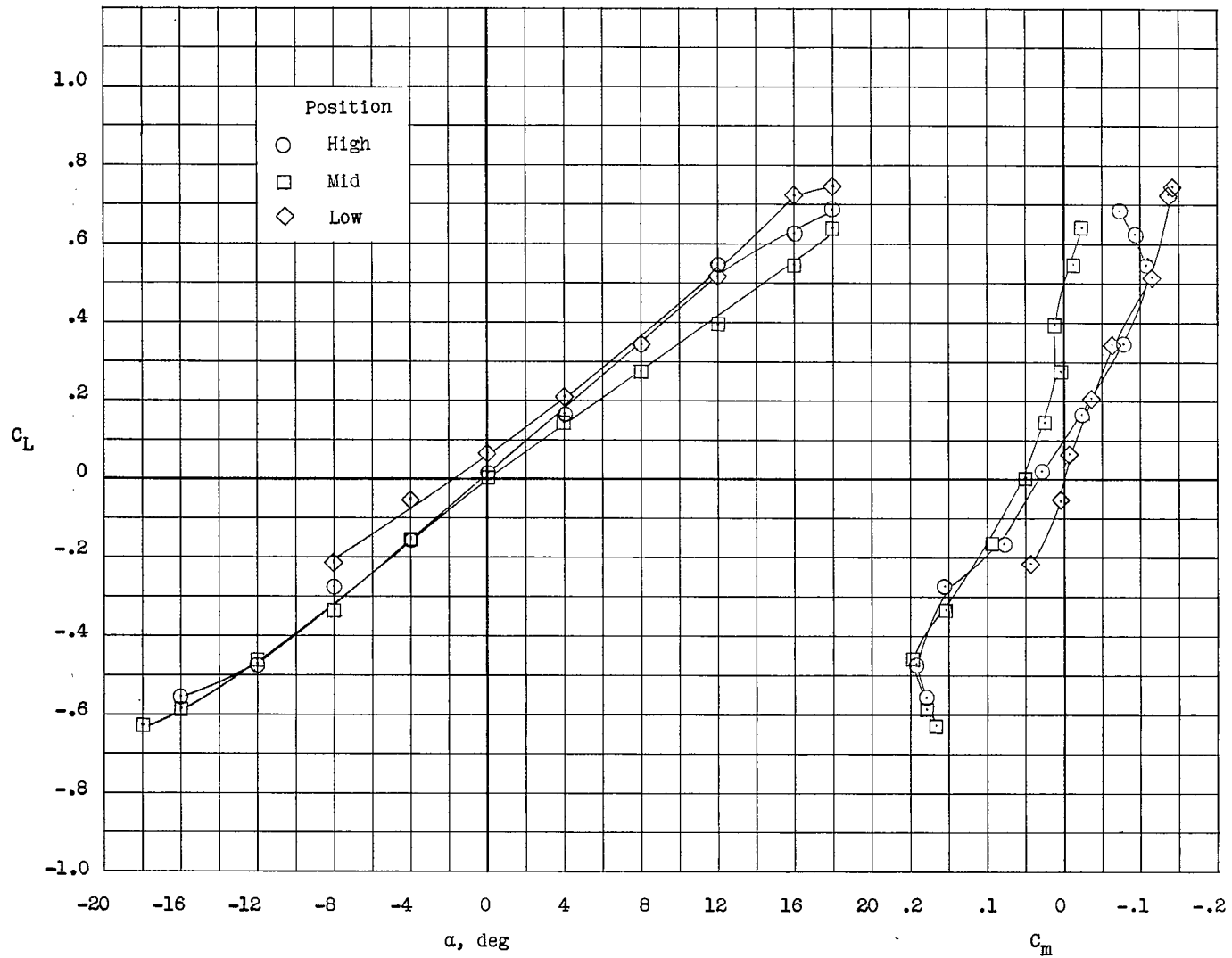


Figure 11.- Longitudinal characteristics of the model with tail 3. $i_w = 0^\circ$; $T'_c = 0$.

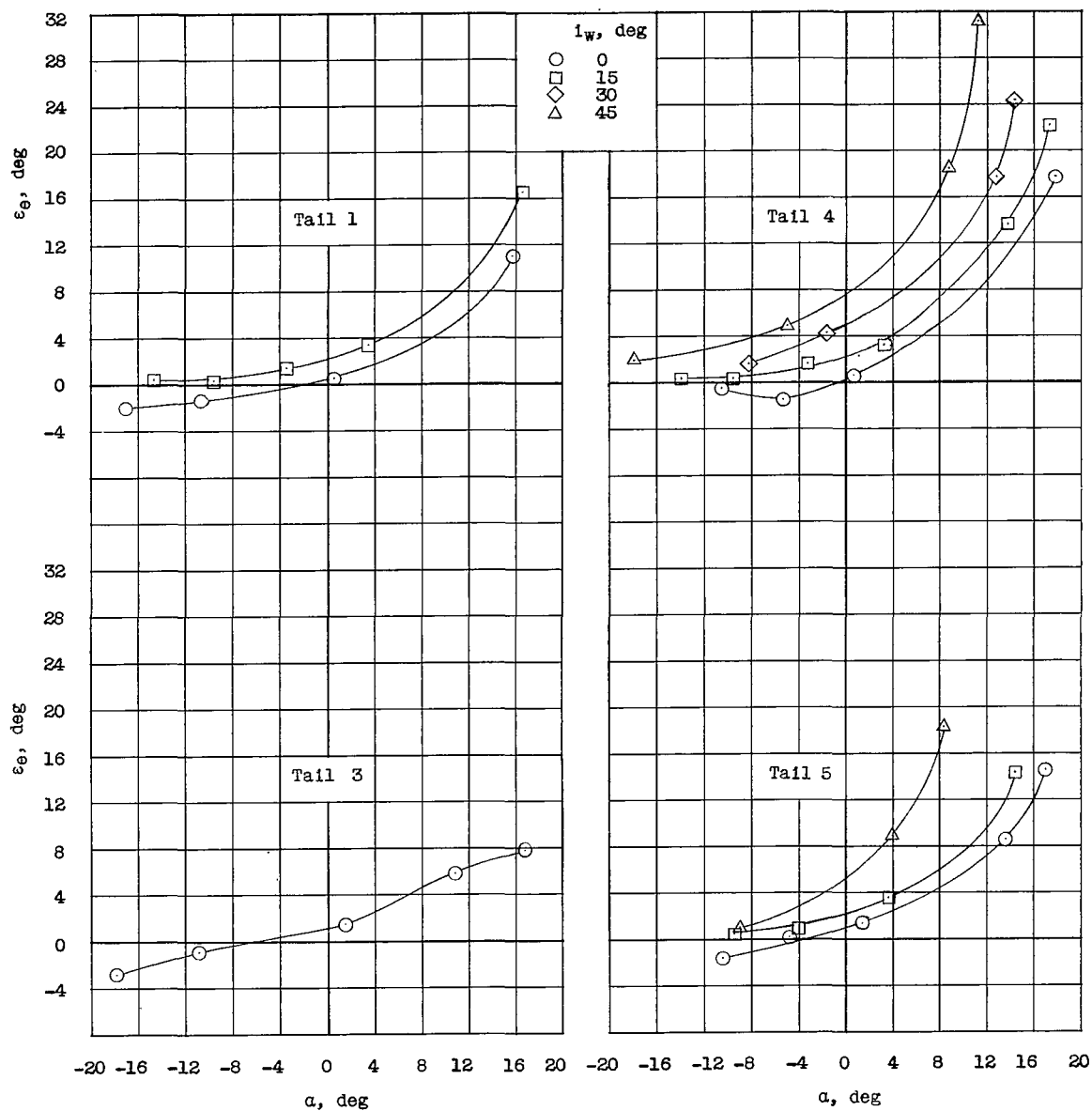


Figure 12.- Variation in the effective downwash angle with angle of attack at wing incidence for tails 1, 4, and 5 in the high position and tail 3 in the mid position.

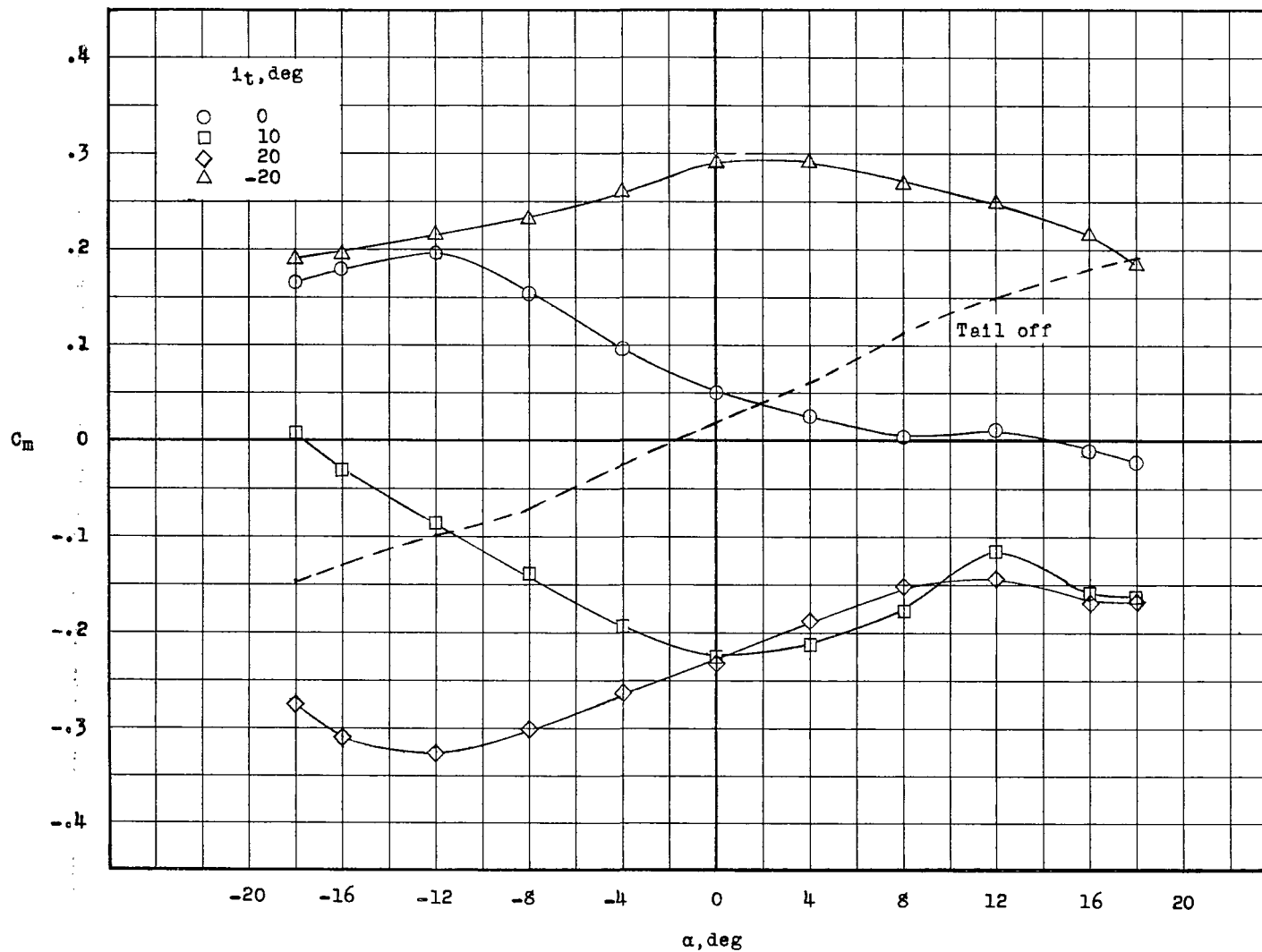
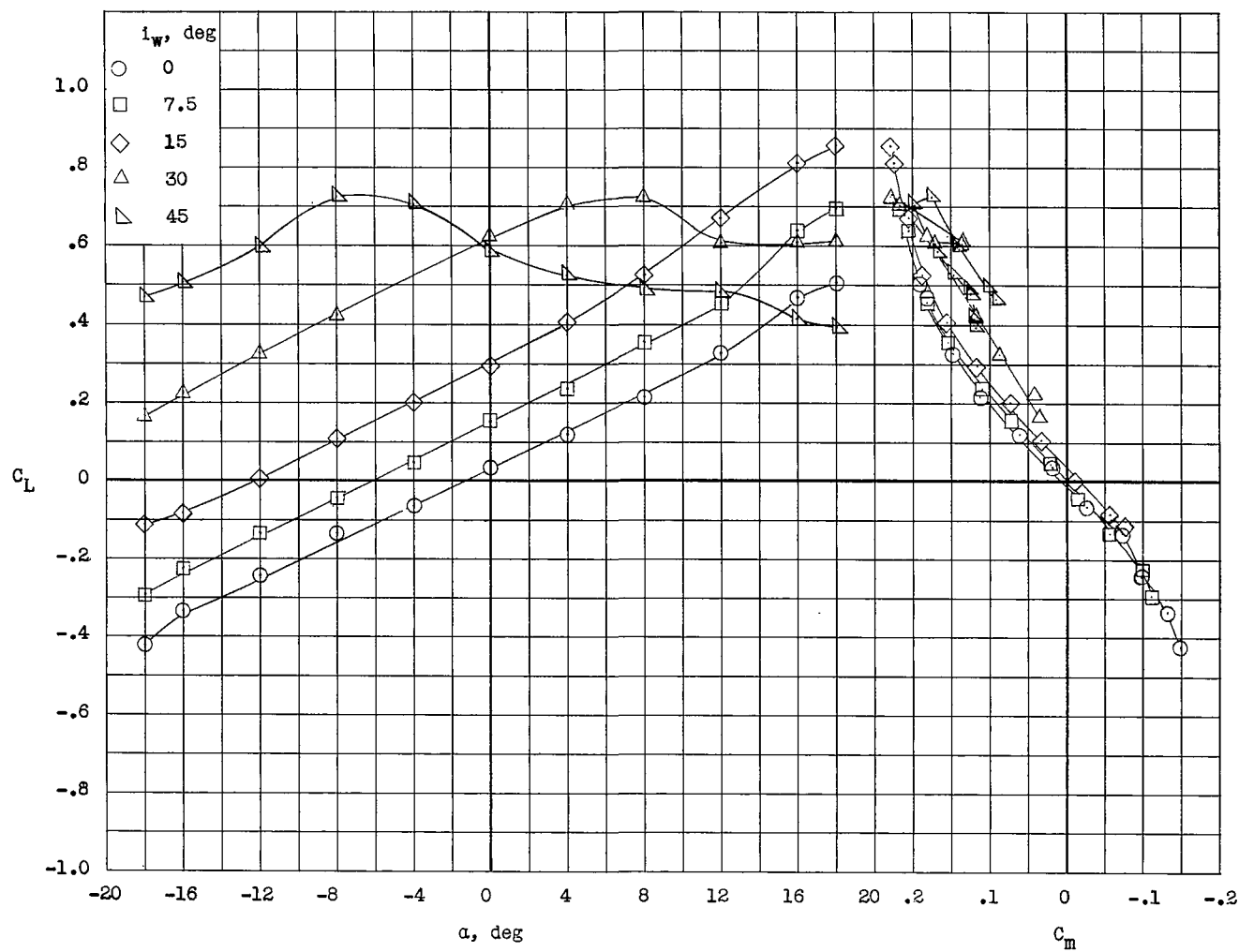
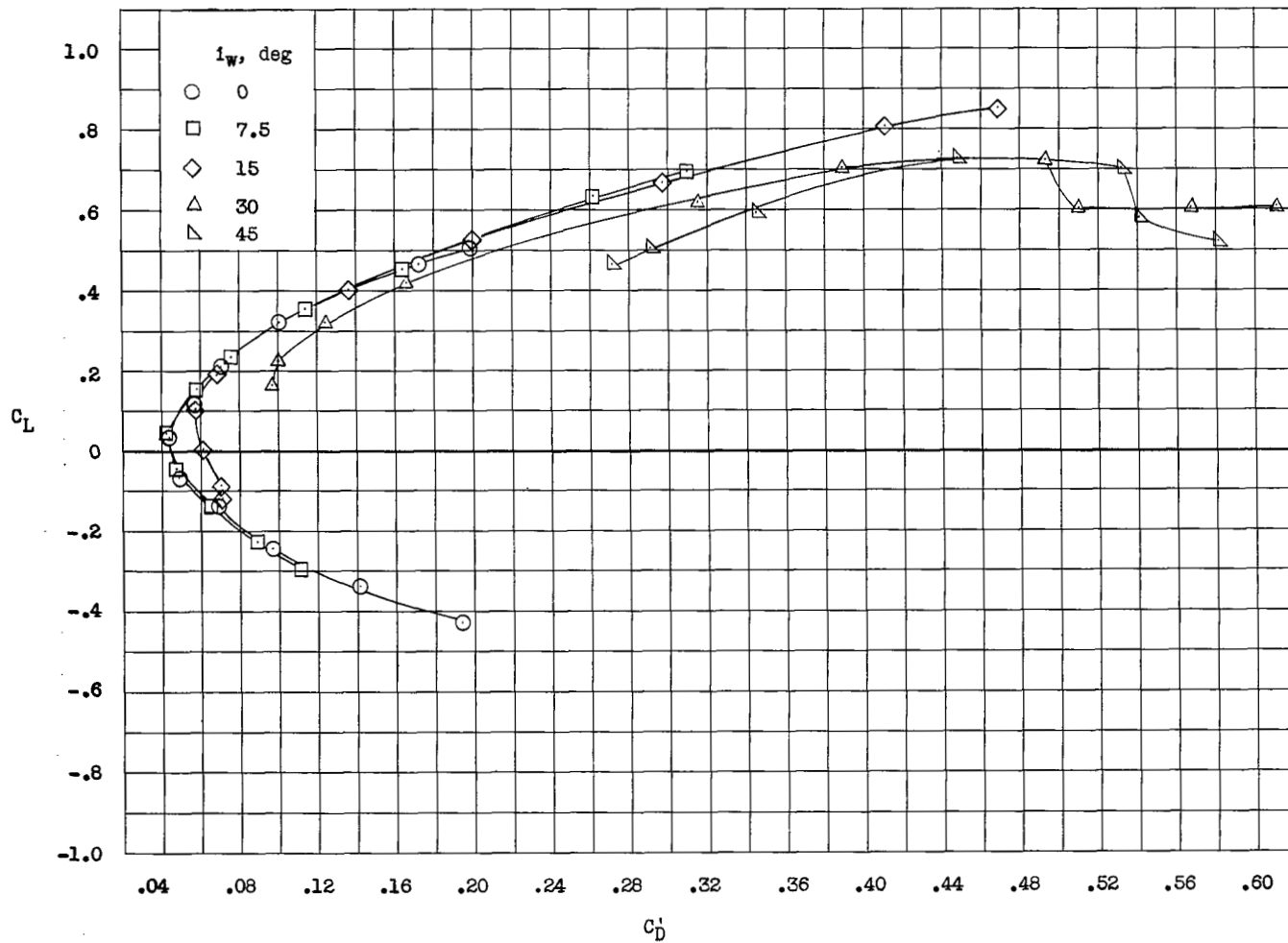


Figure 13.- Variation of pitching-moment coefficient with angle of attack for several horizontal-tail incidence angles. Tail 3; mid position; $i_w = 0^\circ$.



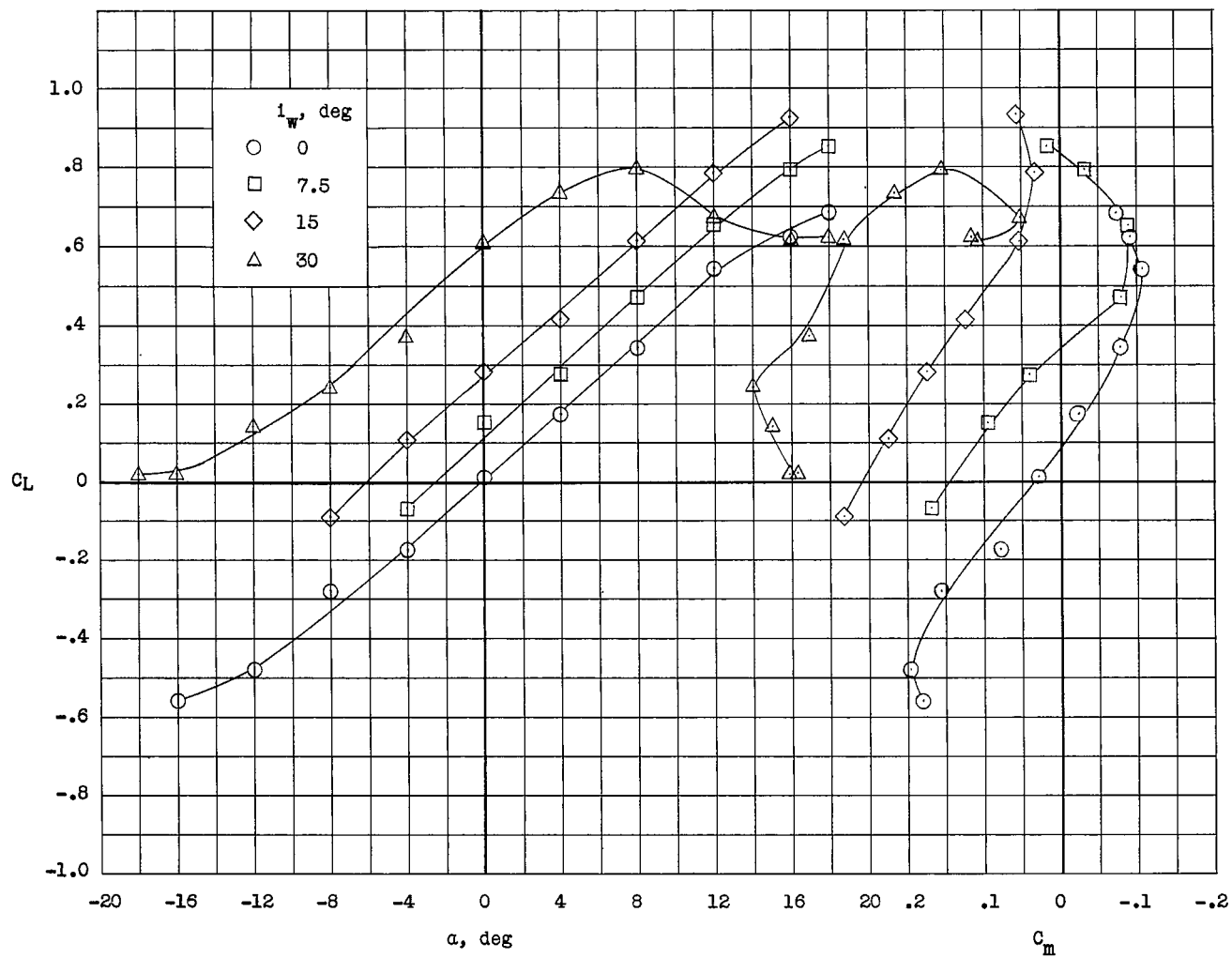
(a) Horizontal tail removed.

Figure 14.- Effect of wing incidence on the longitudinal characteristics of the model. $T'_C = 0$.



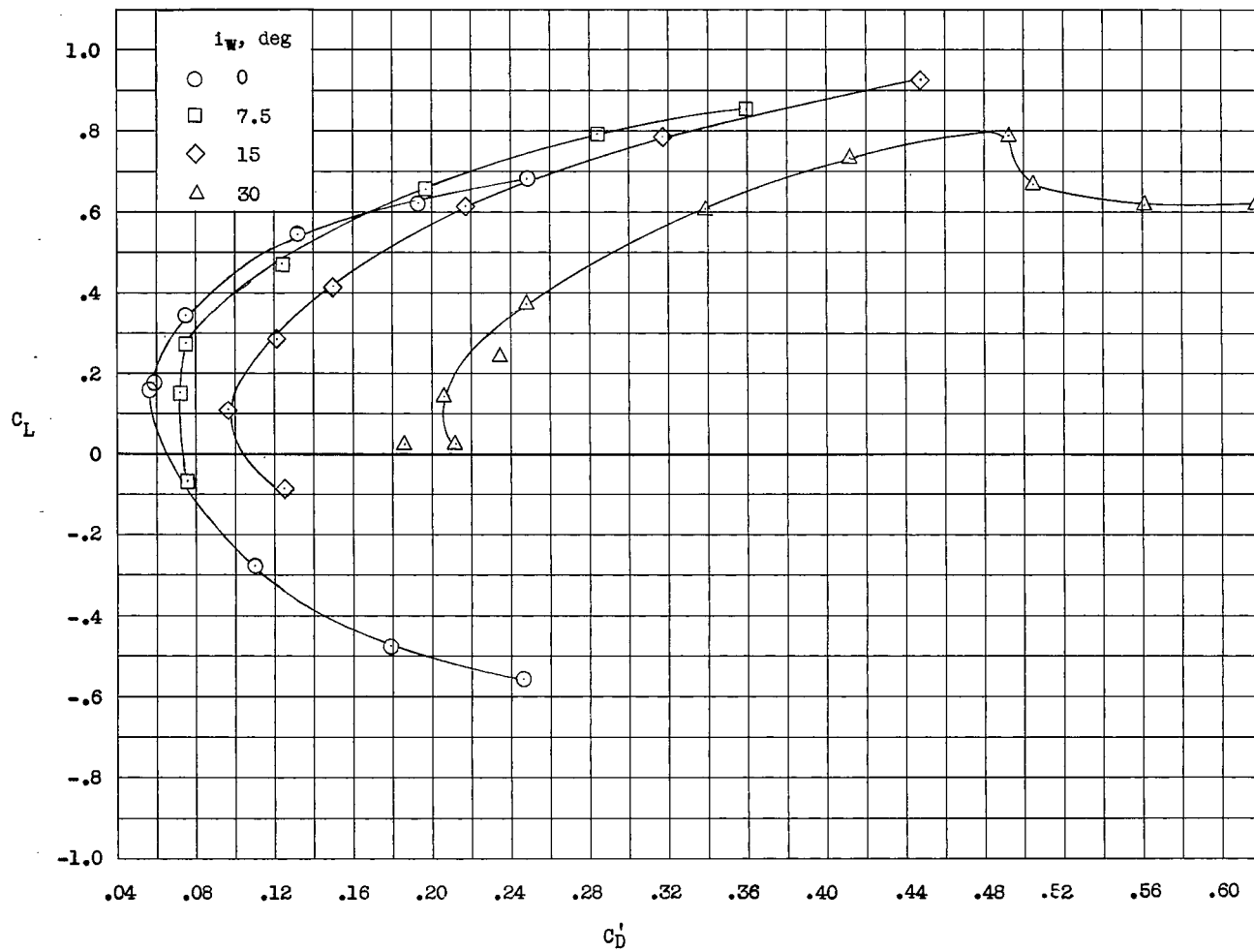
(a) Concluded.

Figure 14.- Continued.



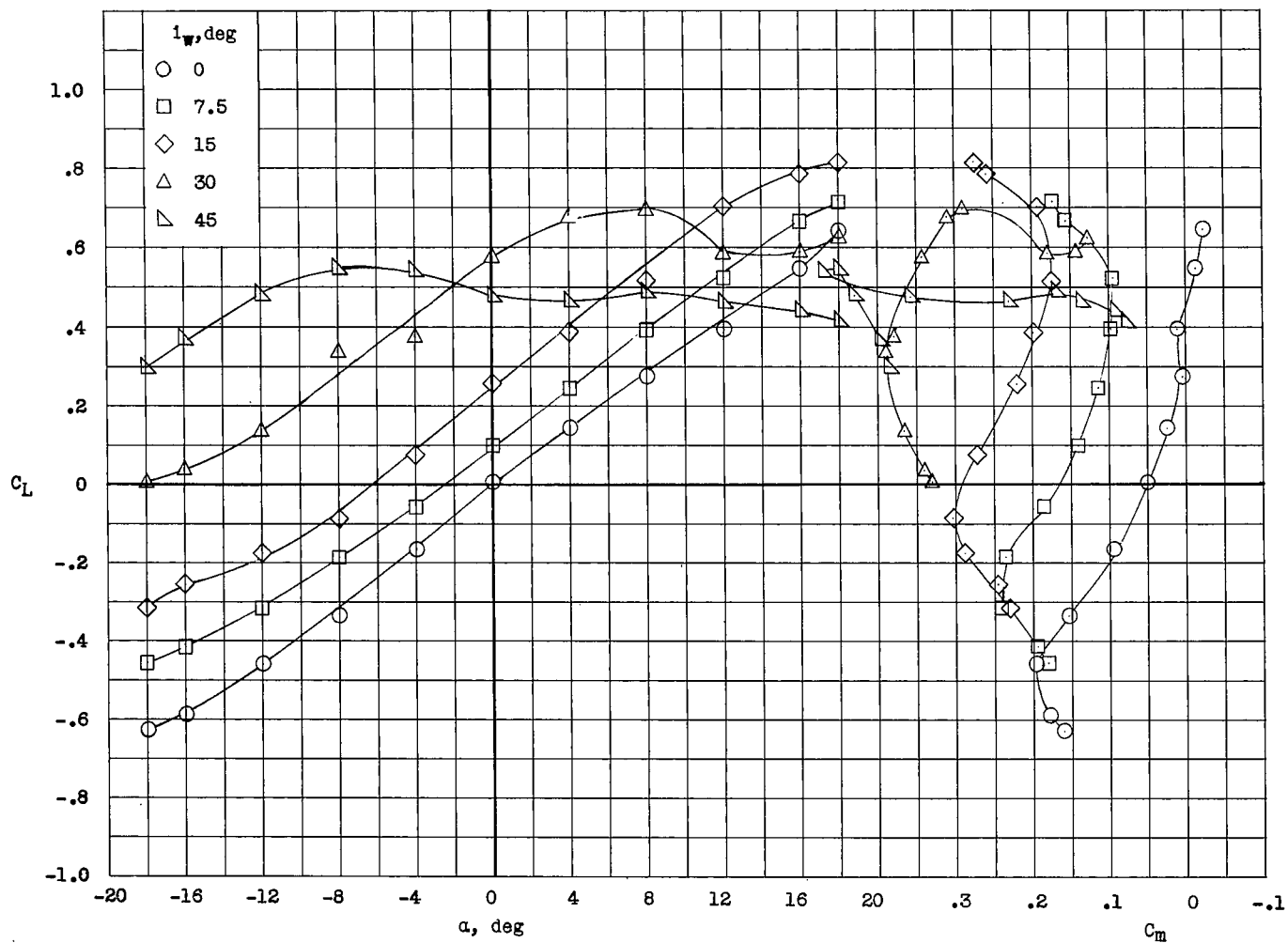
(b) Tail 3; high position.

Figure 14.- Continued.



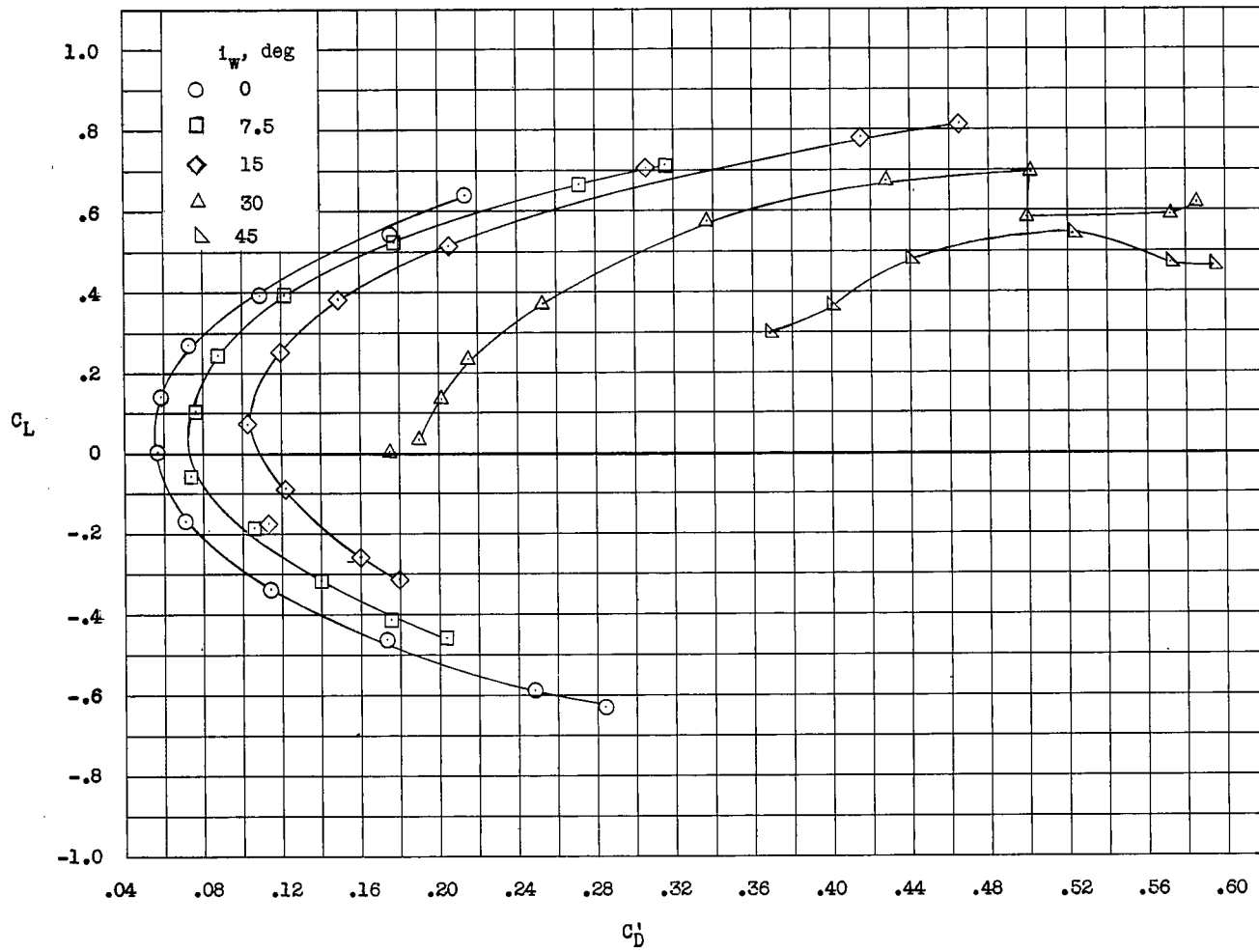
(b) Concluded.

Figure 14.- Continued.



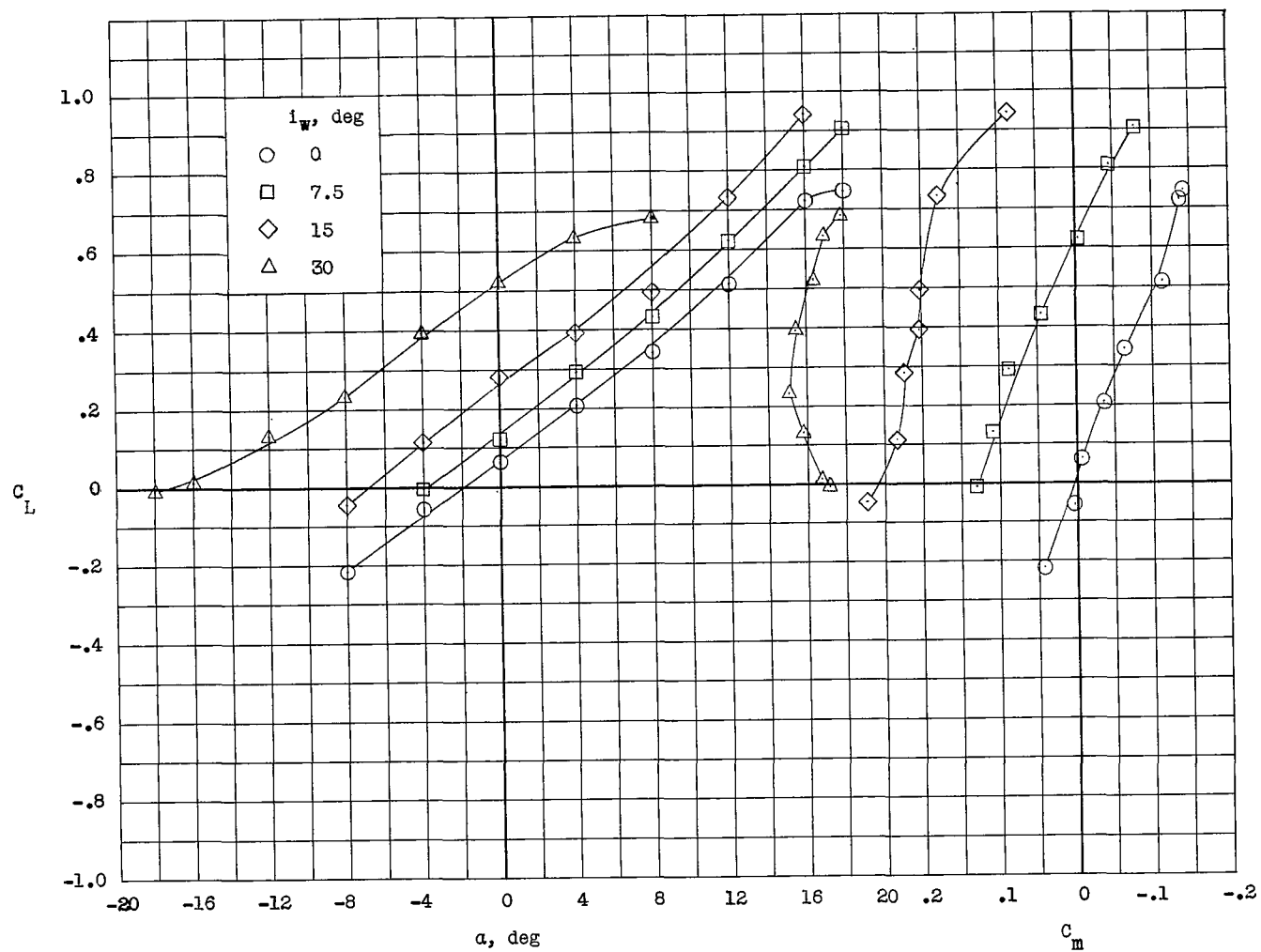
(c) Tail 3; mid position.

Figure 14.- Continued.



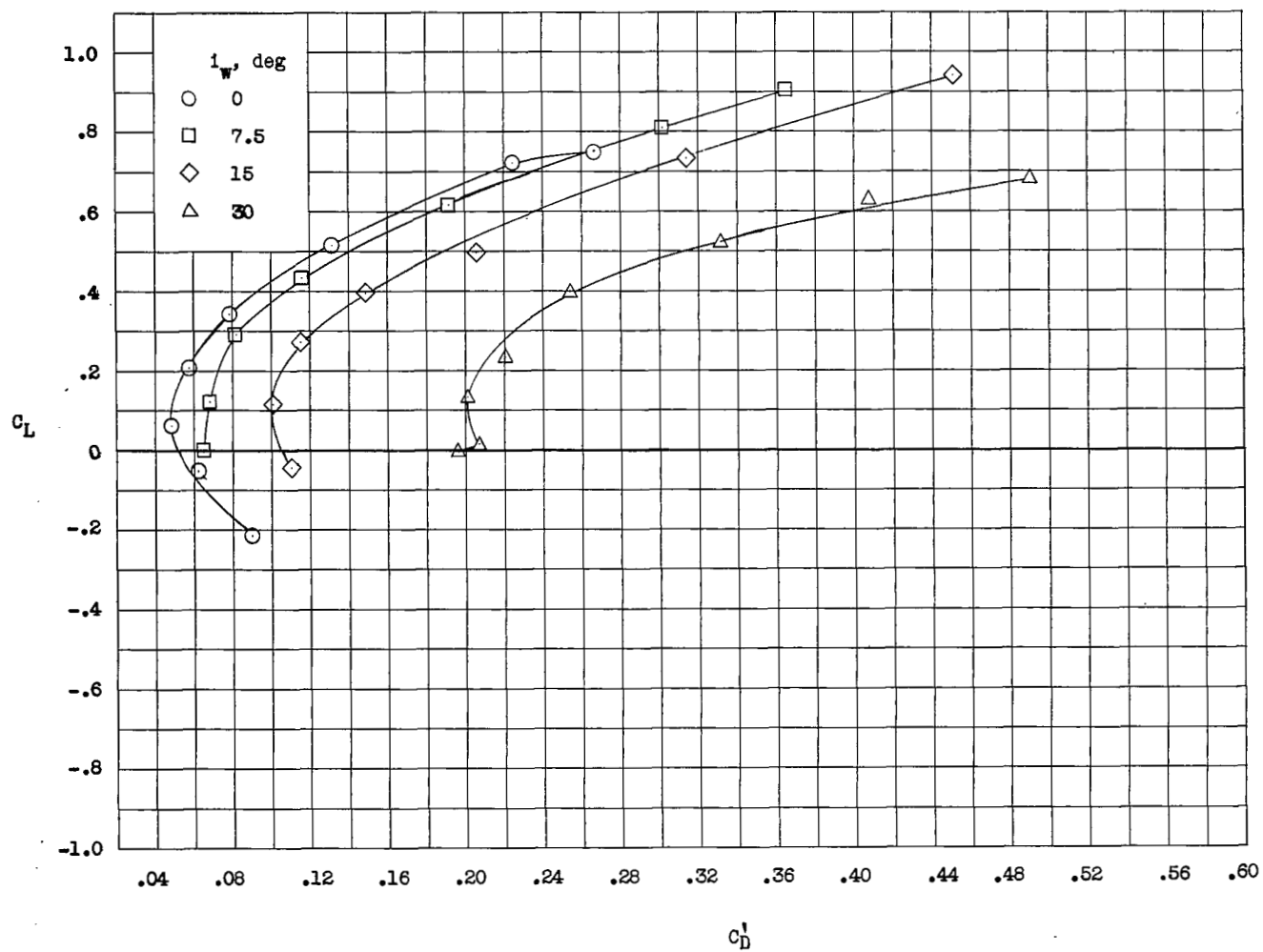
(c) Concluded.

Figure 14.- Continued.



(d) Tail 3; low position.

Figure 14.- Continued.



(d) Concluded.

Figure 14.- Concluded.

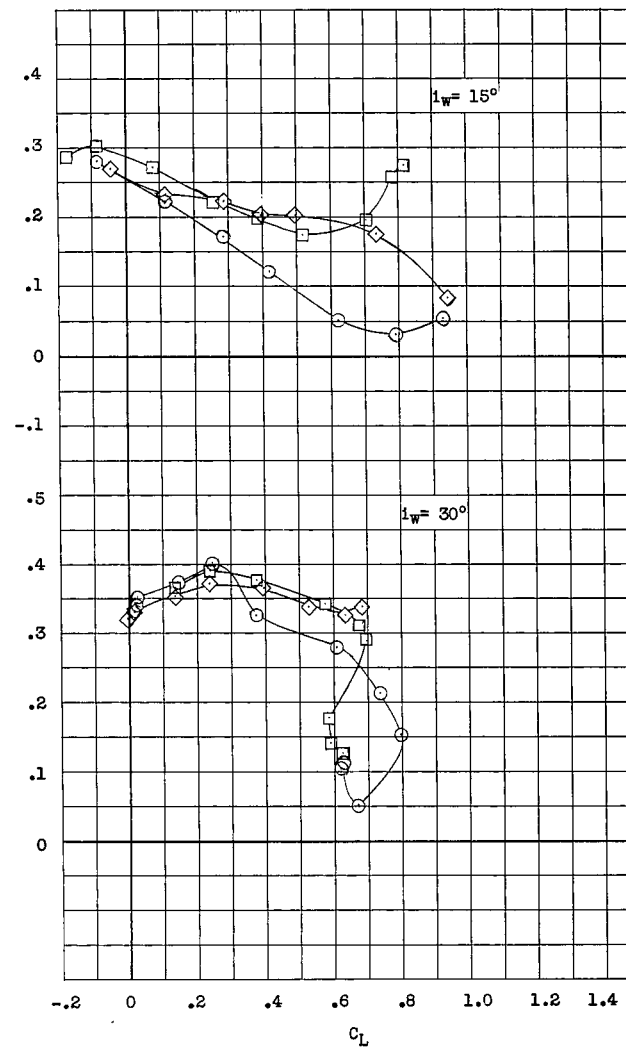
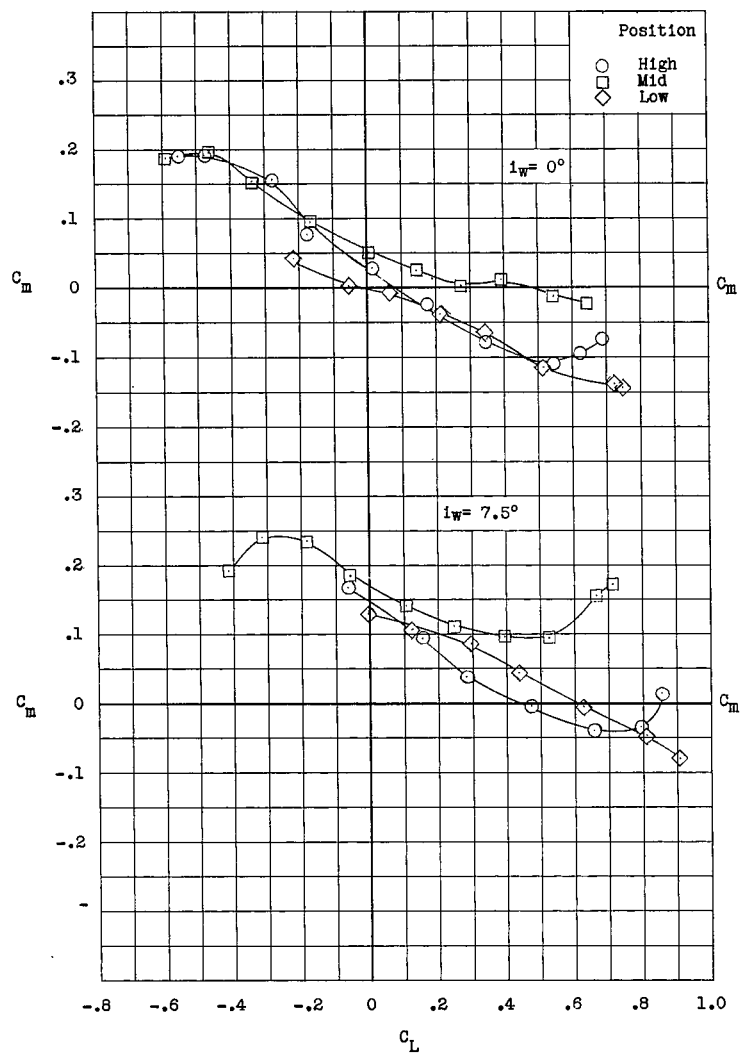
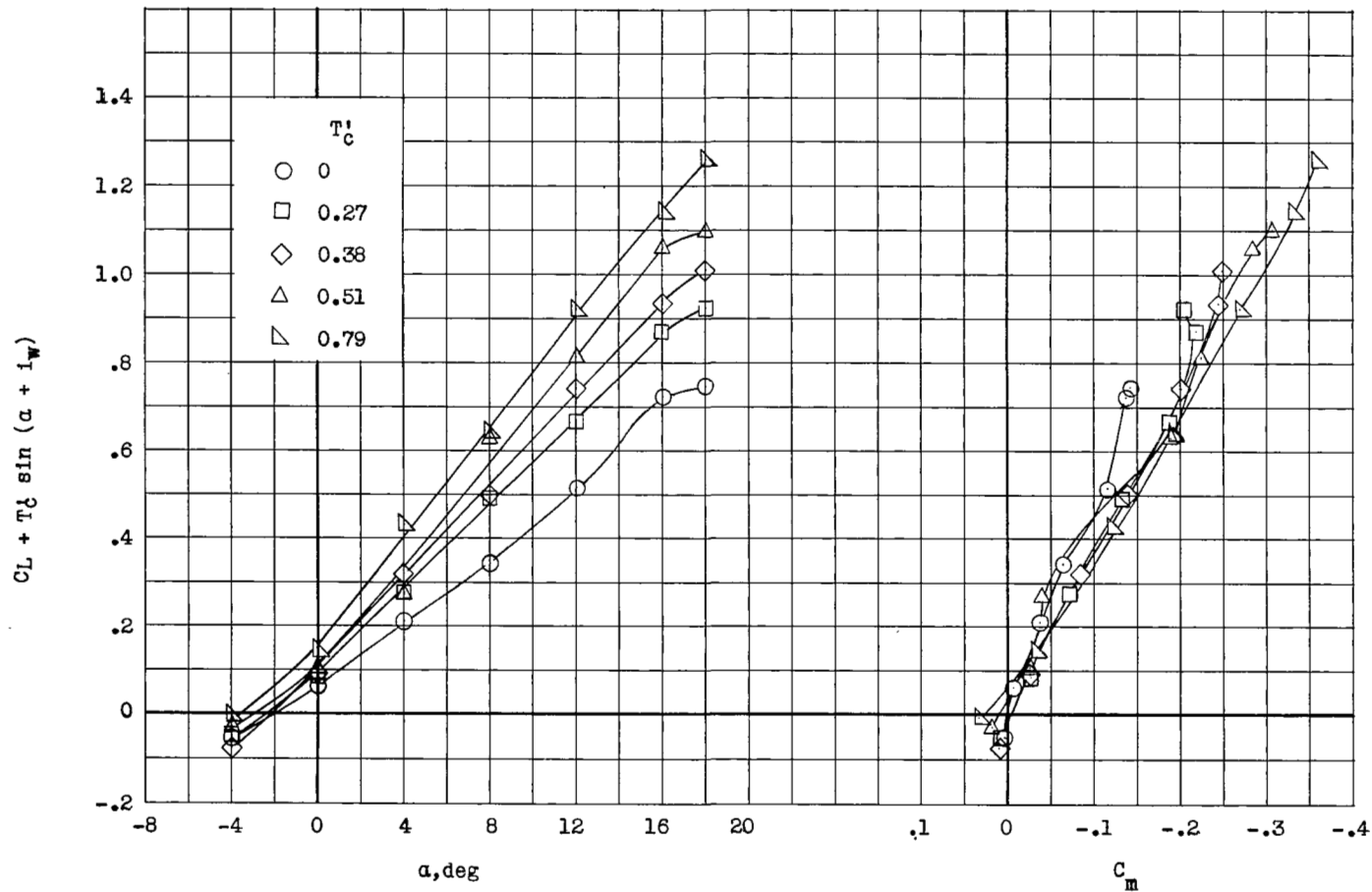
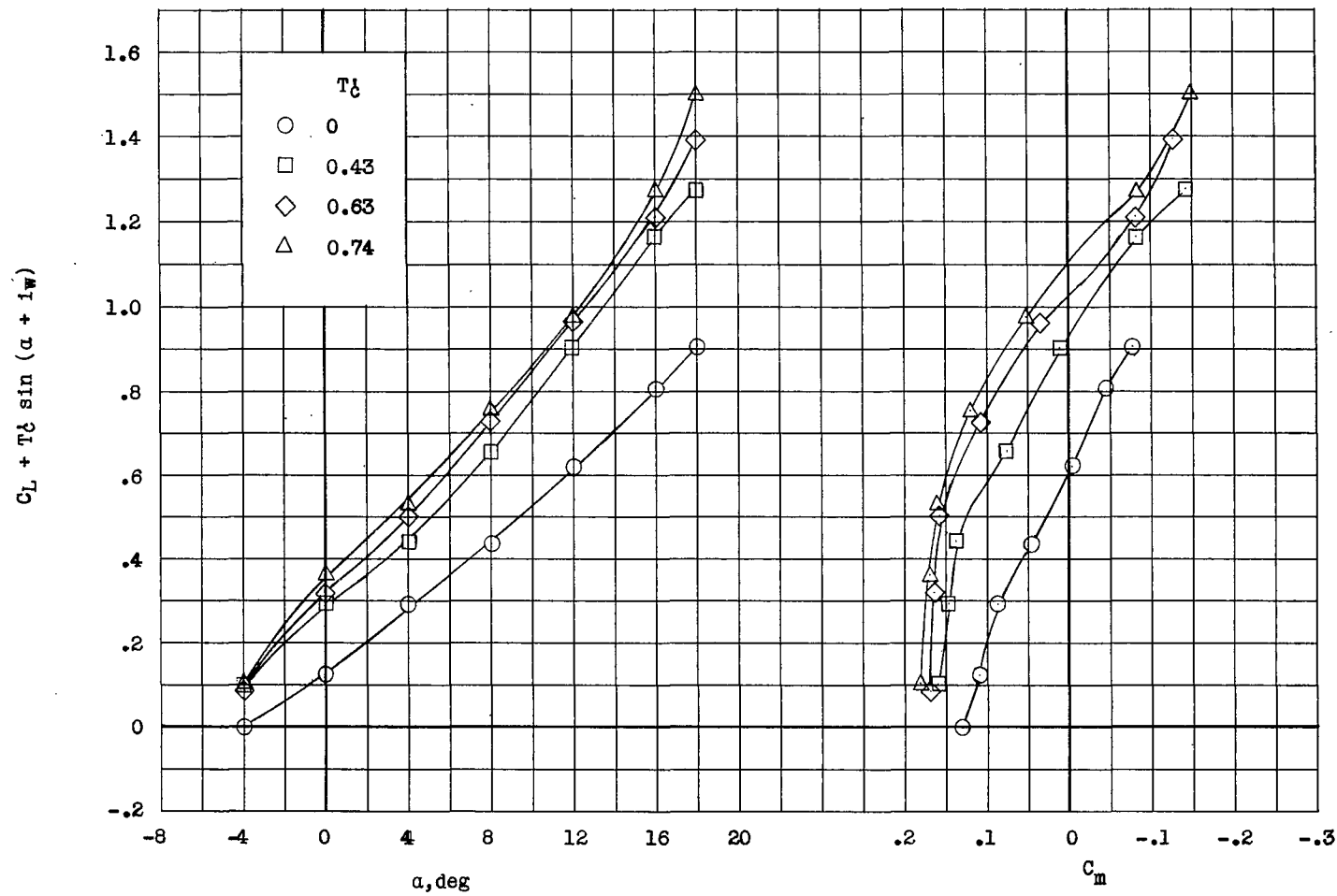


Figure 15.- Summary of the static longitudinal stability characteristics of the model with tail 3. $T'_c = 0$.



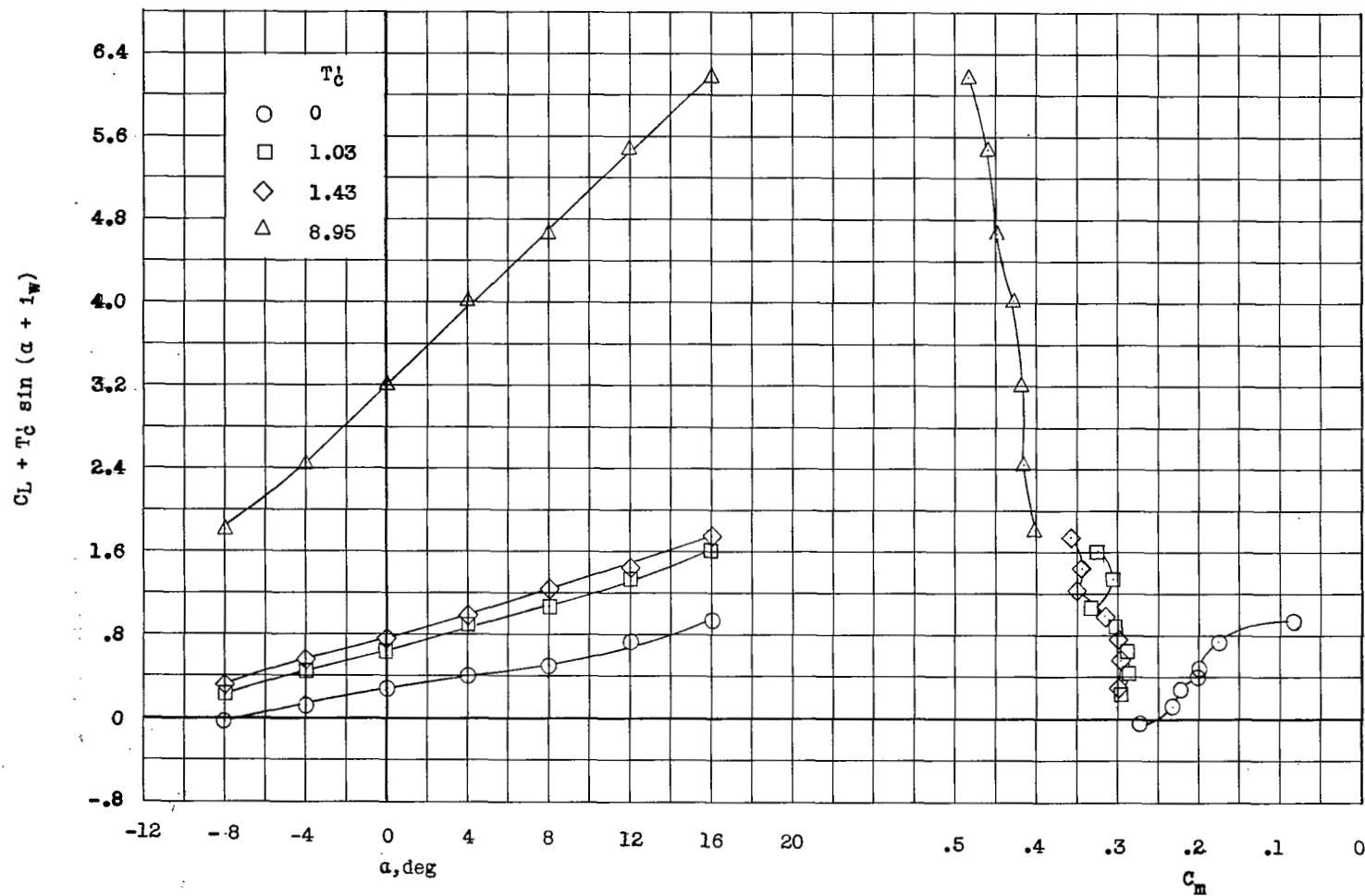
(a) $i_w = 0^\circ$.

Figure 16.- Effect of T'_c on the lift and pitching-moment characteristics of the model with tail 3 in the low position. $\delta_j = 0^\circ$.



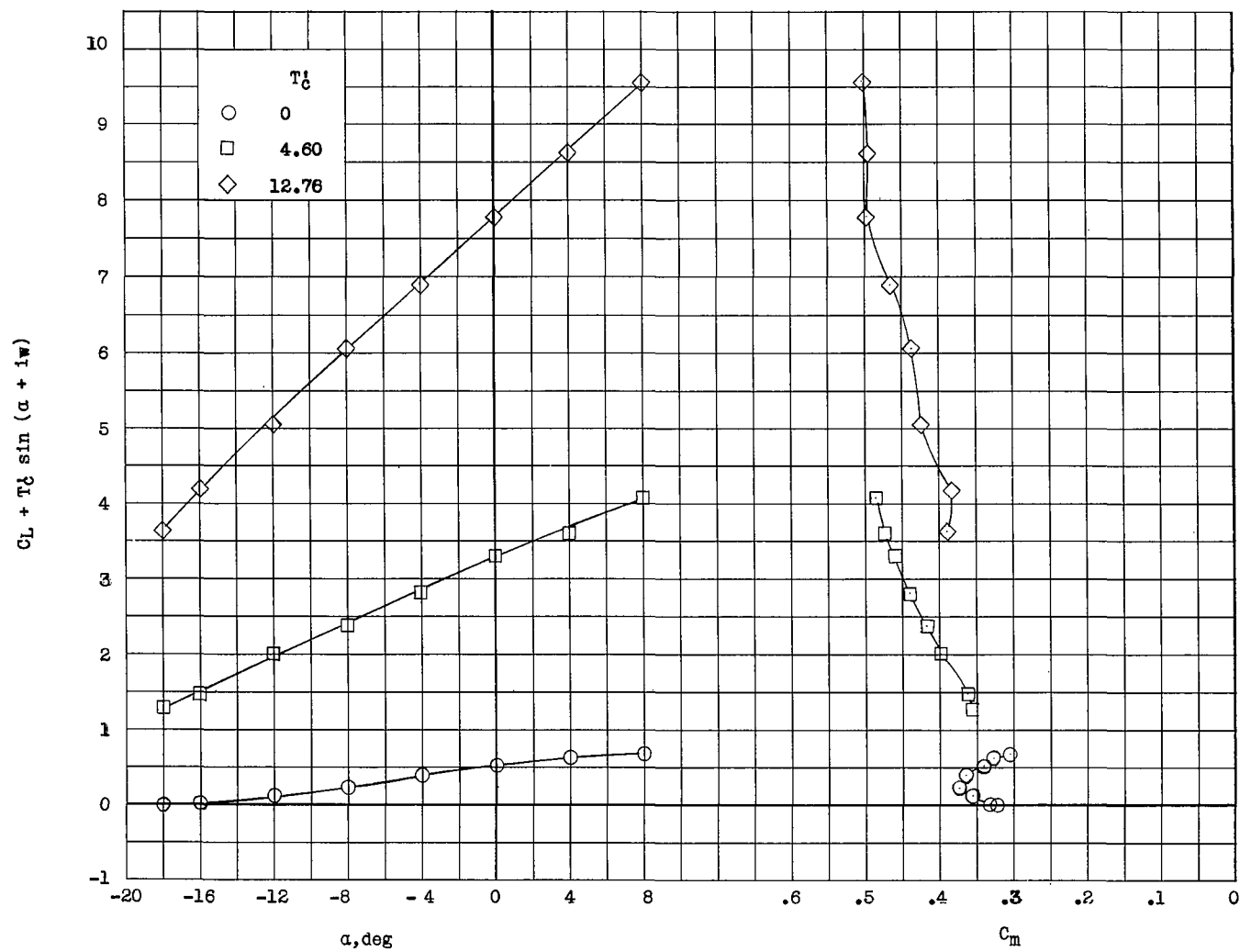
(b) $i_w = 7.5^\circ$.

Figure 16.- Continued.



(c) $i_w = 15^\circ$.

Figure 16.- Continued.



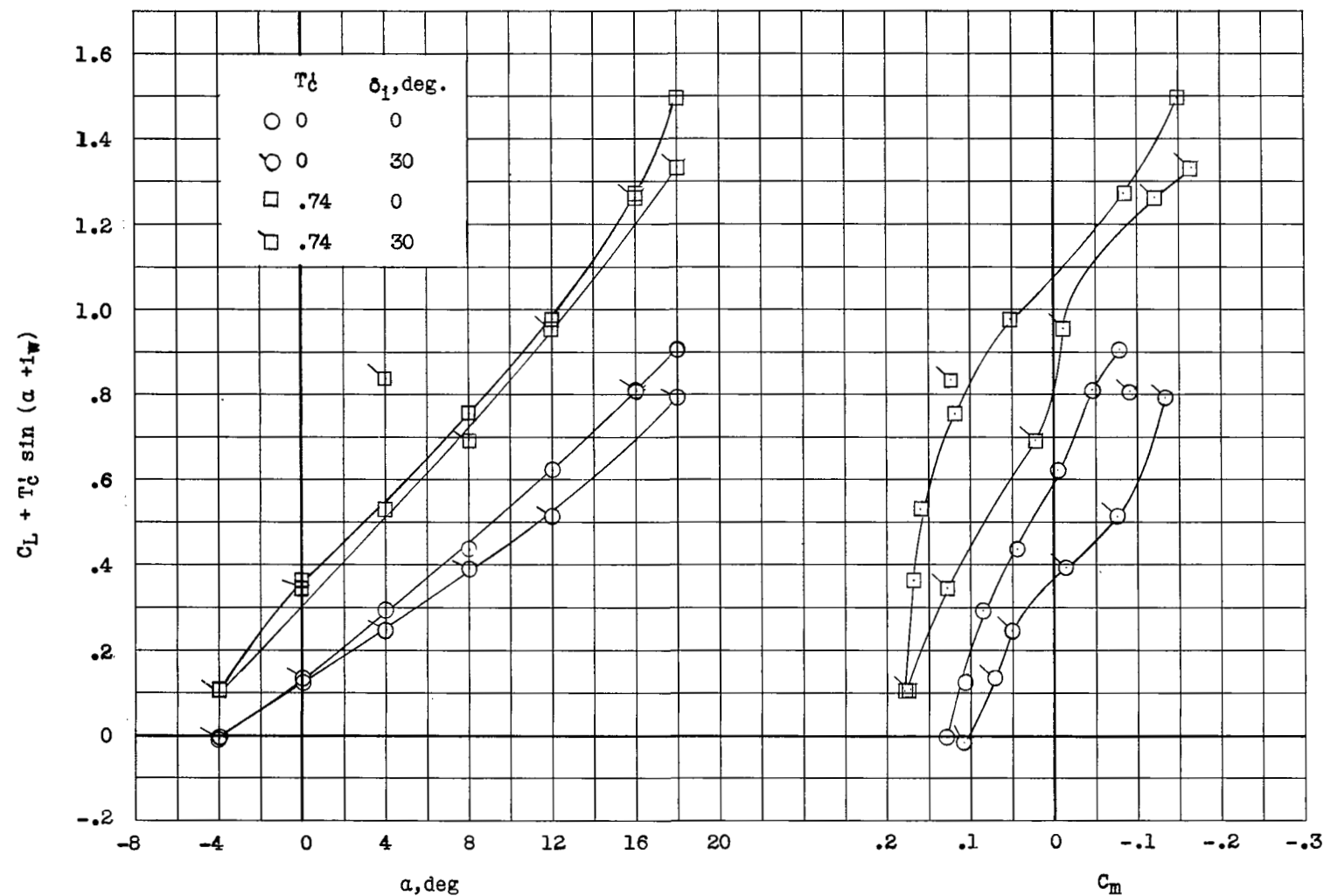


Figure 17.- Effect of T'_c and δ_1 on the lift and pitching-moment characteristics of the model with tail 3 in the low position. $i_w = 7.5^\circ$.

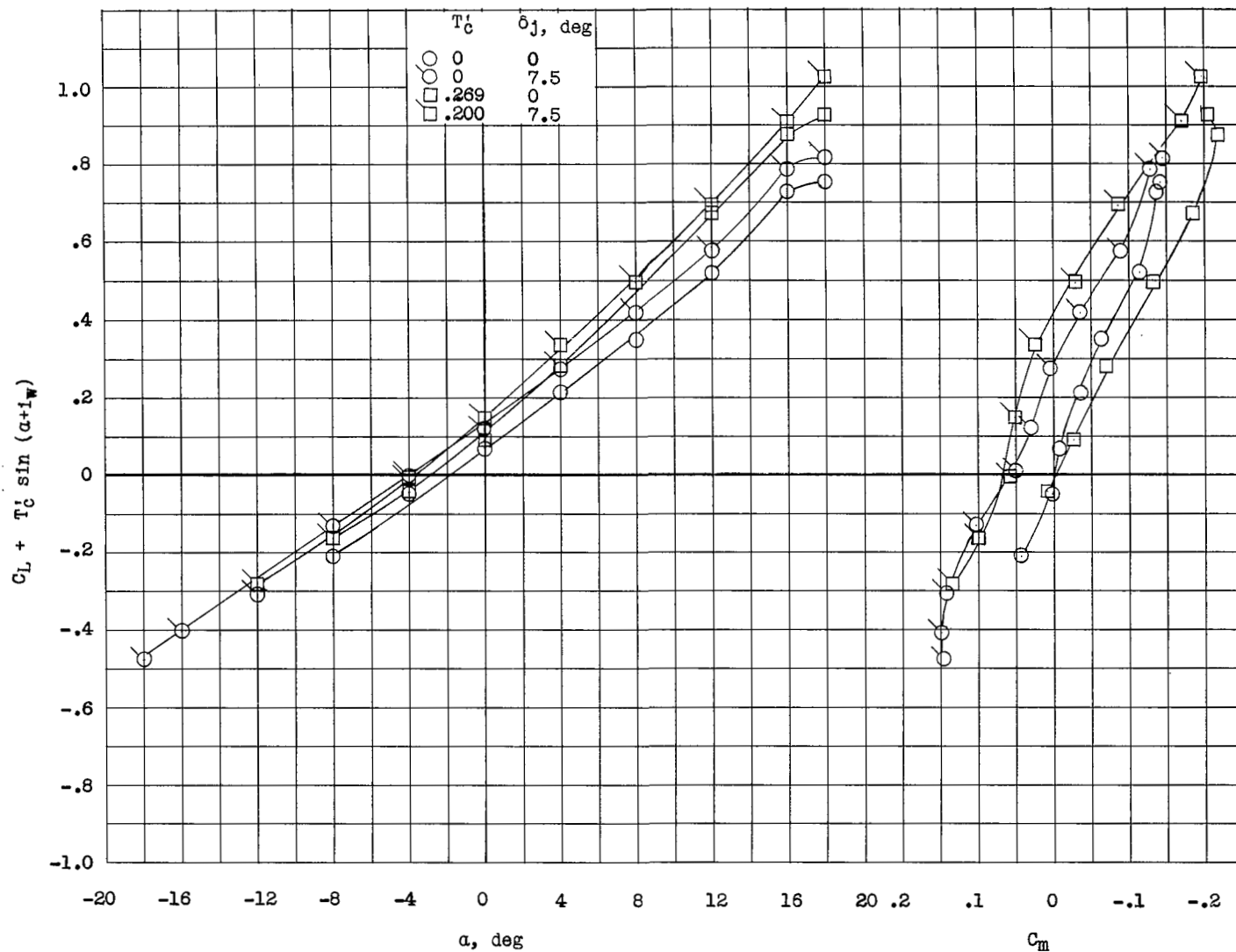
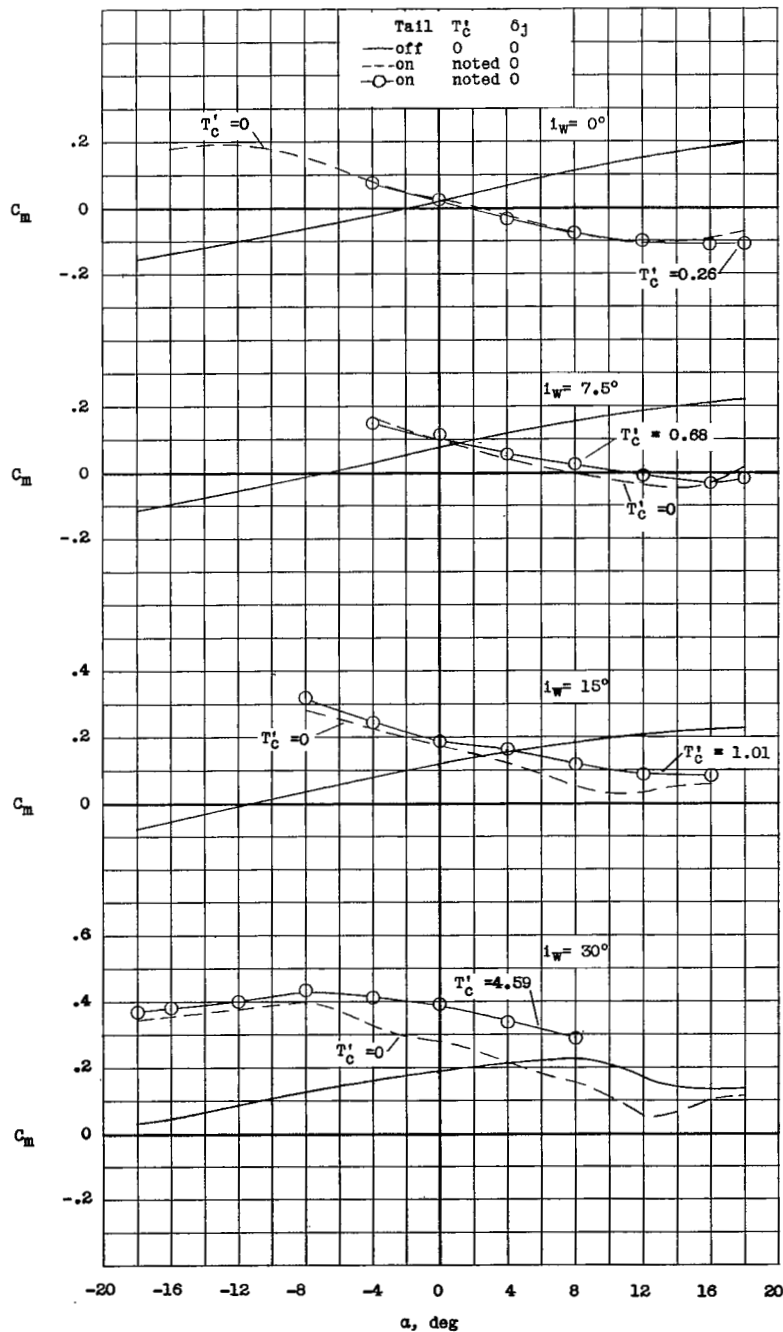
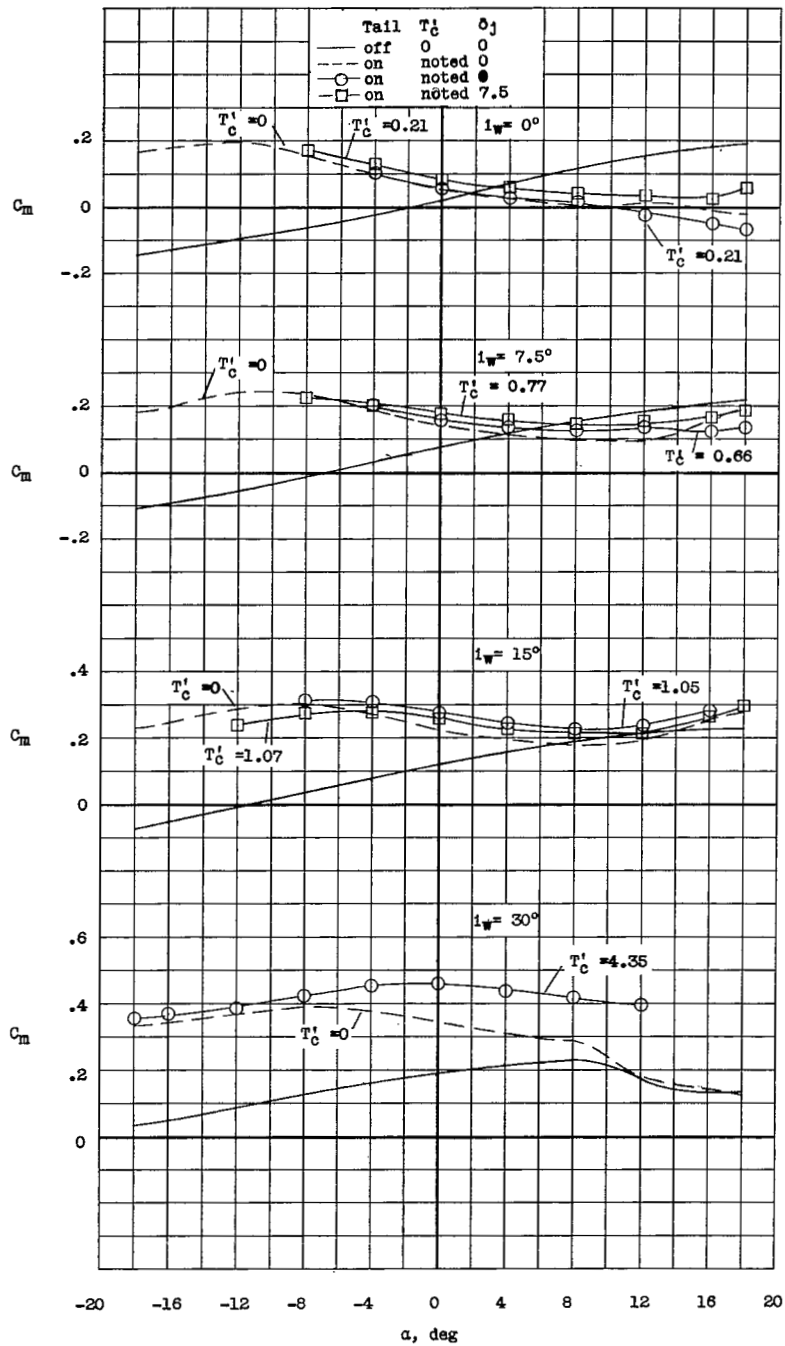


Figure 18.- Effect of jet deflection on the longitudinal characteristics of the model with the large tail in the low position. $i_w = 0^\circ$.



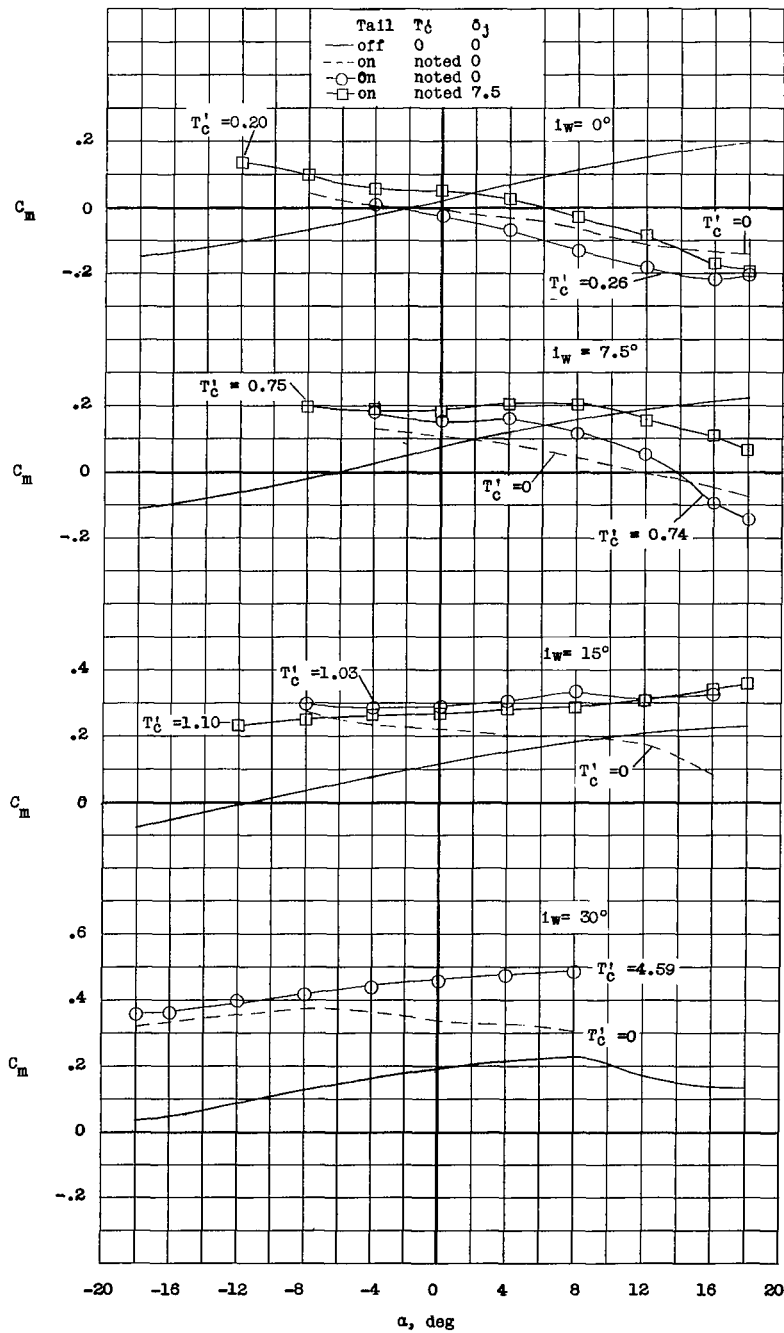
(a) Tail 3; high position.

Figure 19.- Summary of the static longitudinal stability characteristics of the model at several thrust coefficients.



(b) Tail 3; mid position.

Figure 19.- Continued.



(c) Tail 3; low position.

Figure 19.- Concluded.

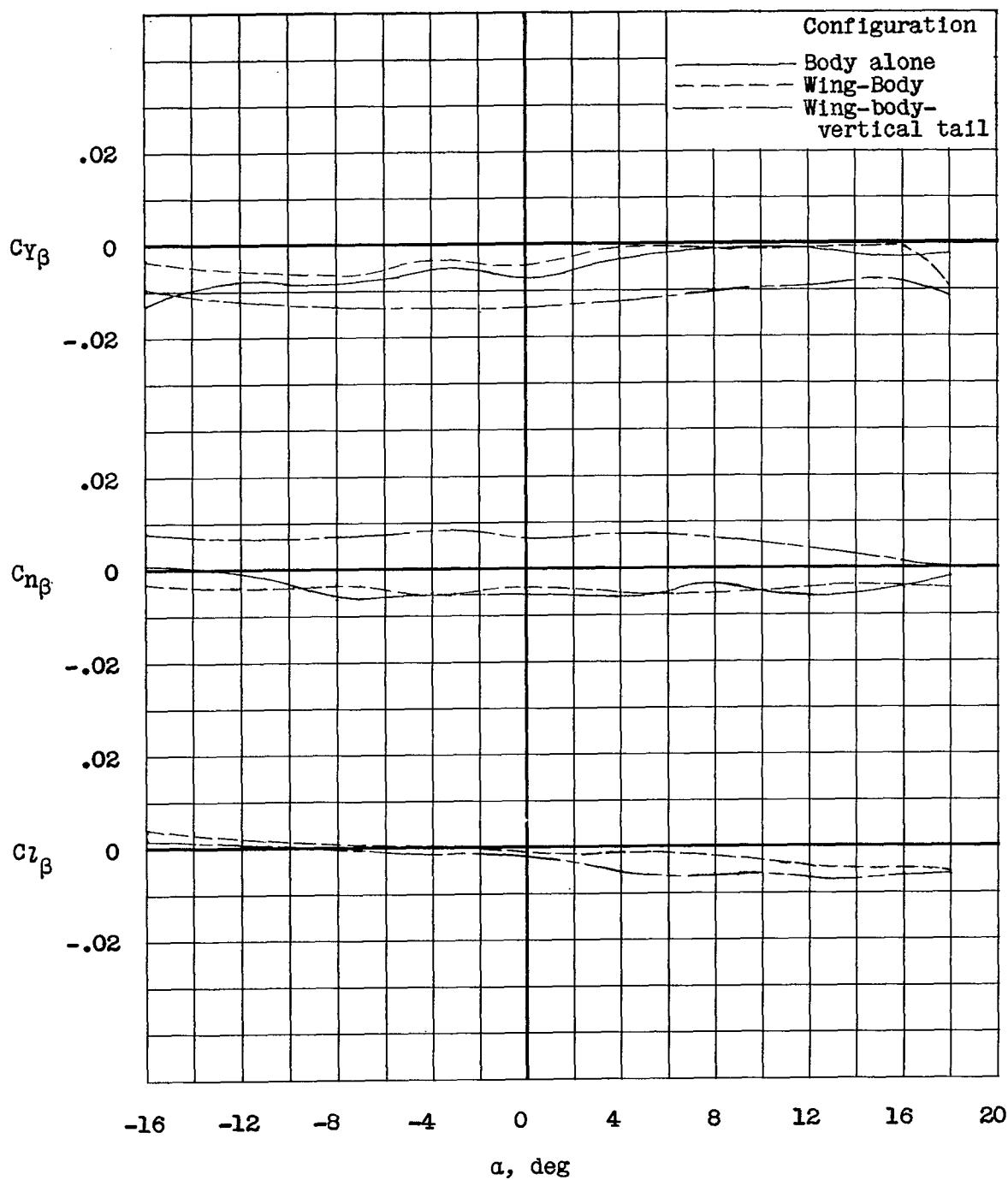
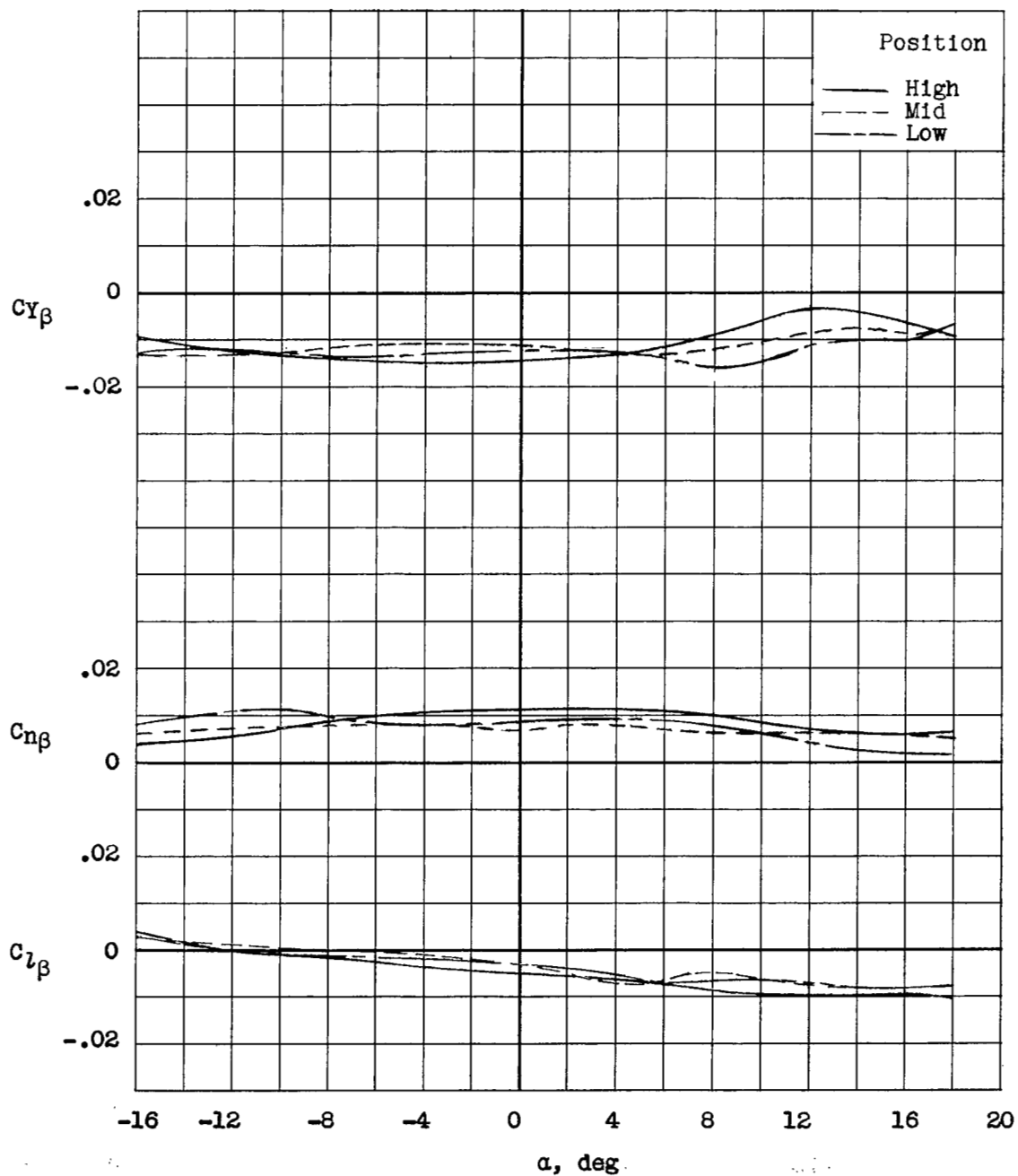
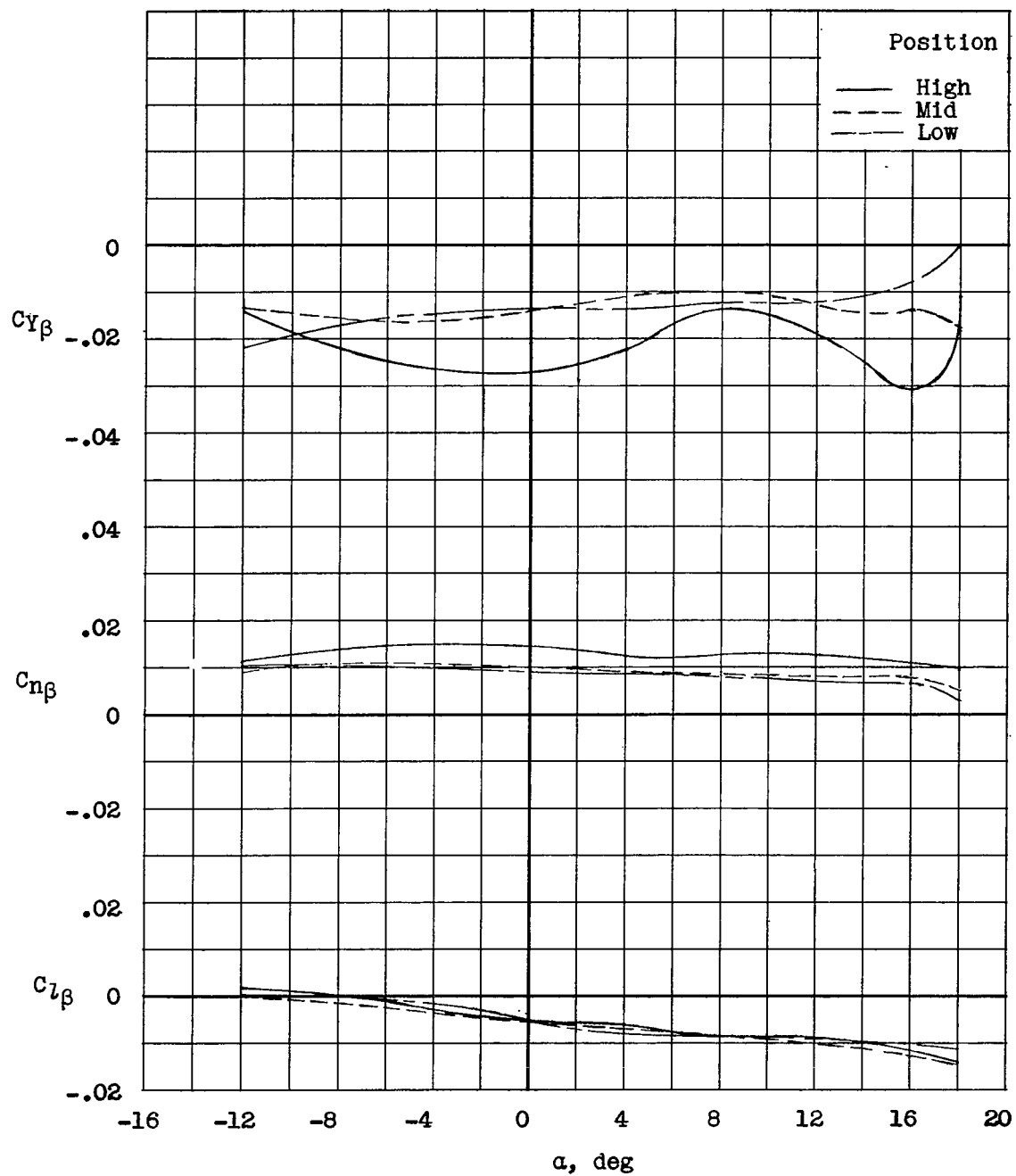


Figure 20.- Static lateral and directional characteristics of the model without a horizontal tail. Tailpipes deflected 7.5° ; $i_w = 0^\circ$.



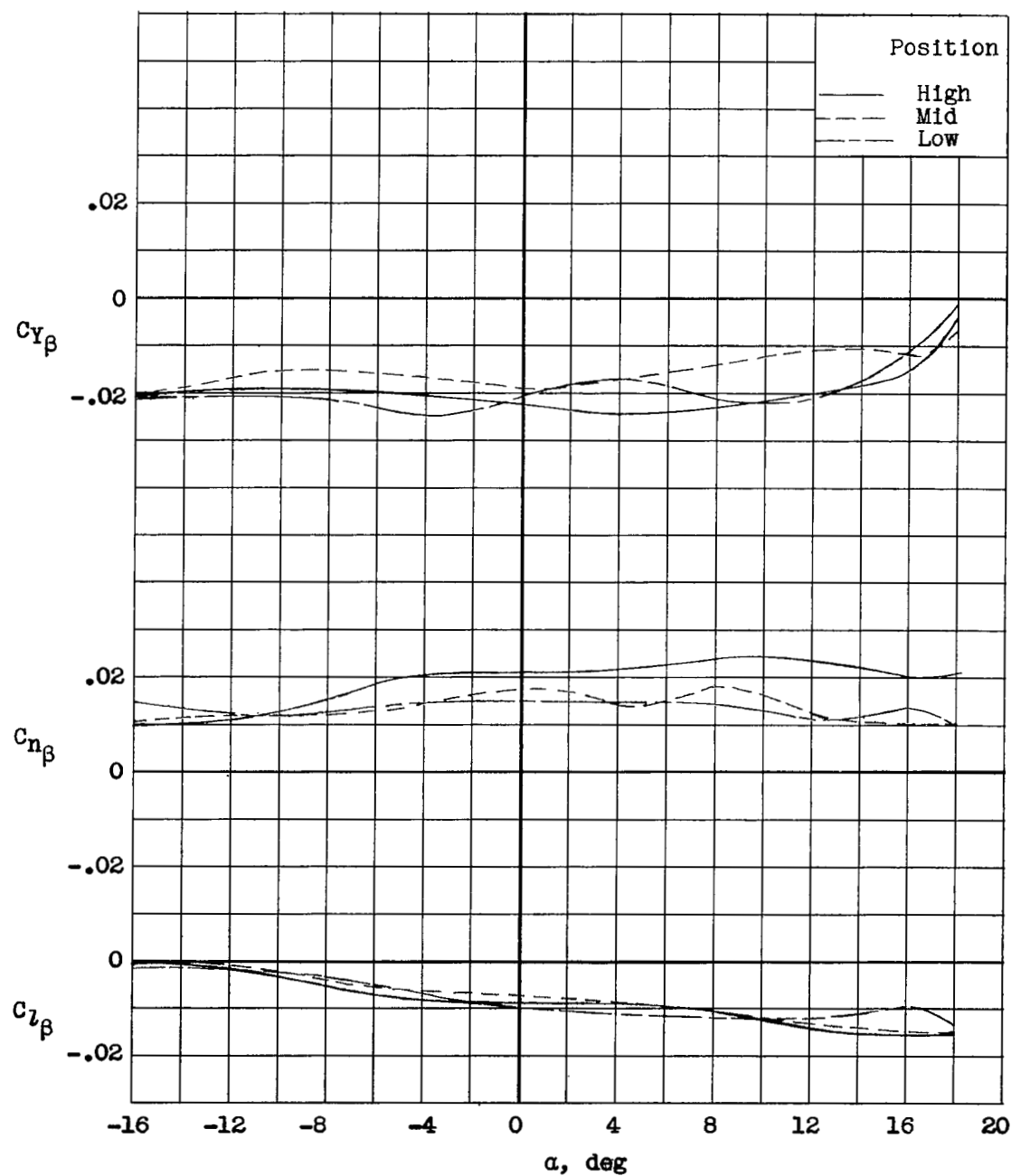
(a) $i_w = 0^\circ$; $T'_c = 0$.

Figure 21.- Static lateral and directional characteristics of the model with tail 3. $\delta_j = 7.5^\circ$.



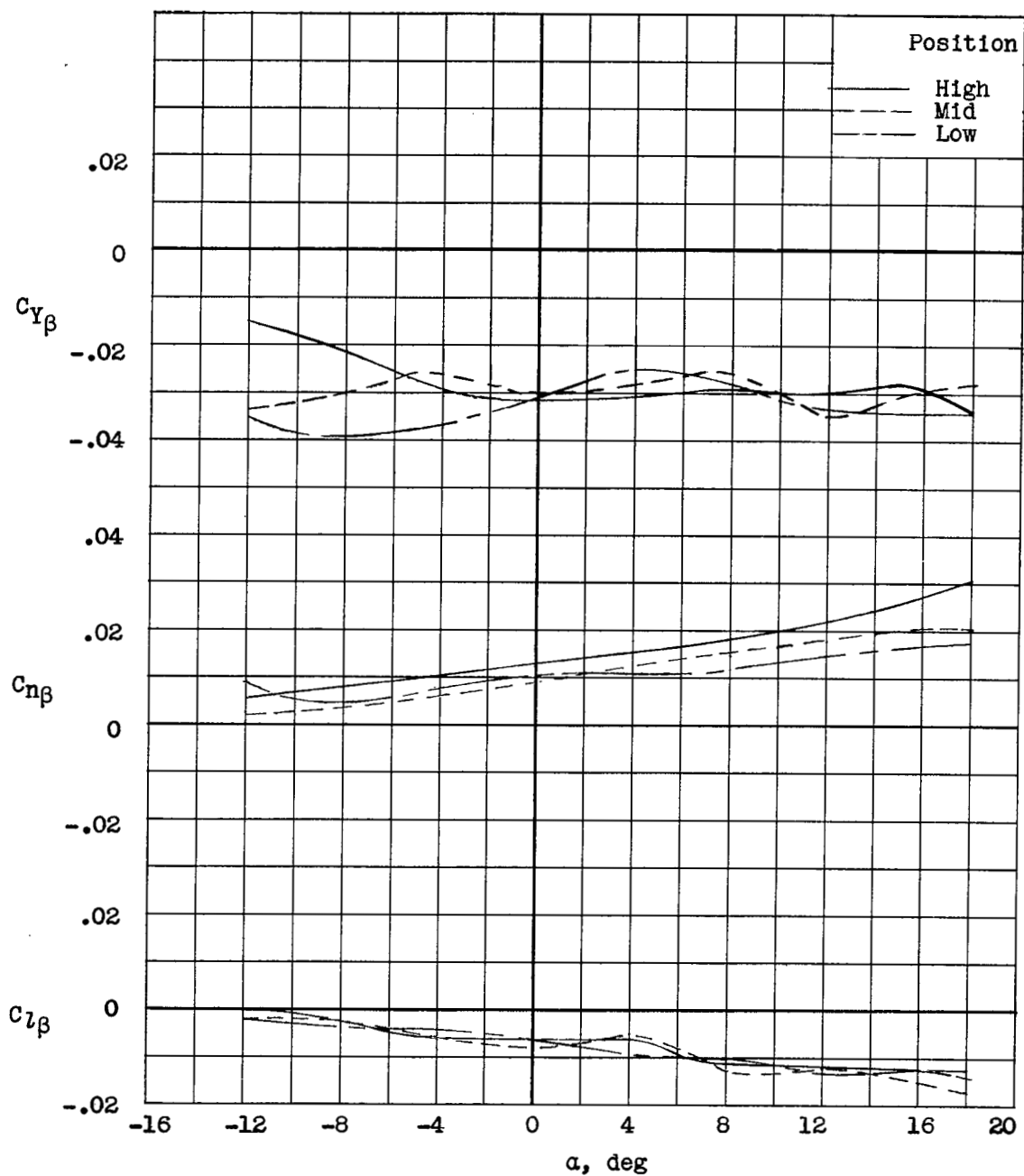
(b) $i_w = 0^\circ$; $T'_c = 0.190$.

Figure 21.- Continued.



(c) $i_w = 15^\circ$; $T'_c = 0$.

Figure 21.- Continued.



(d) $i_w = 15^\circ$; $T'_c = 1.00$.

Figure 21.- Concluded.

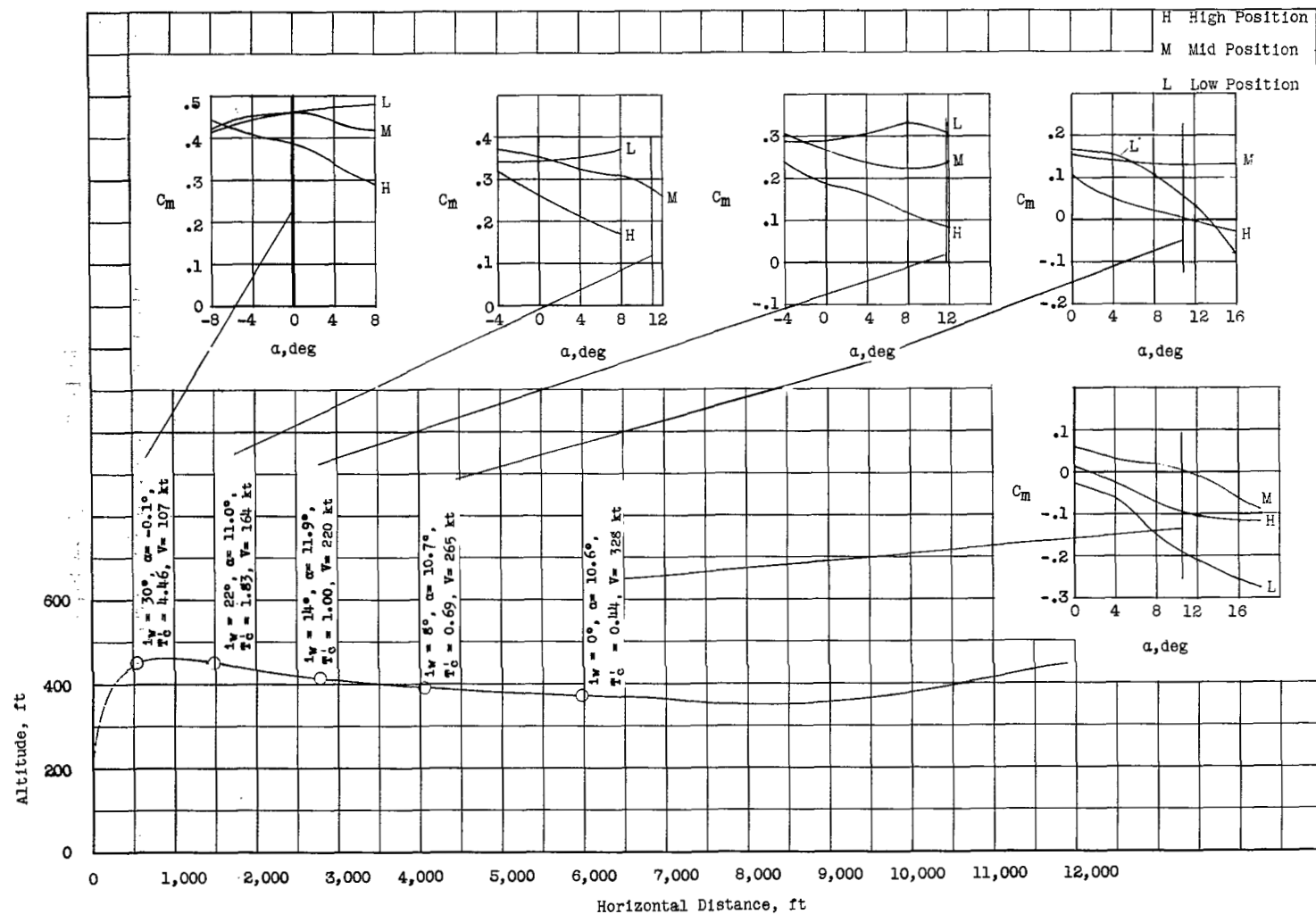
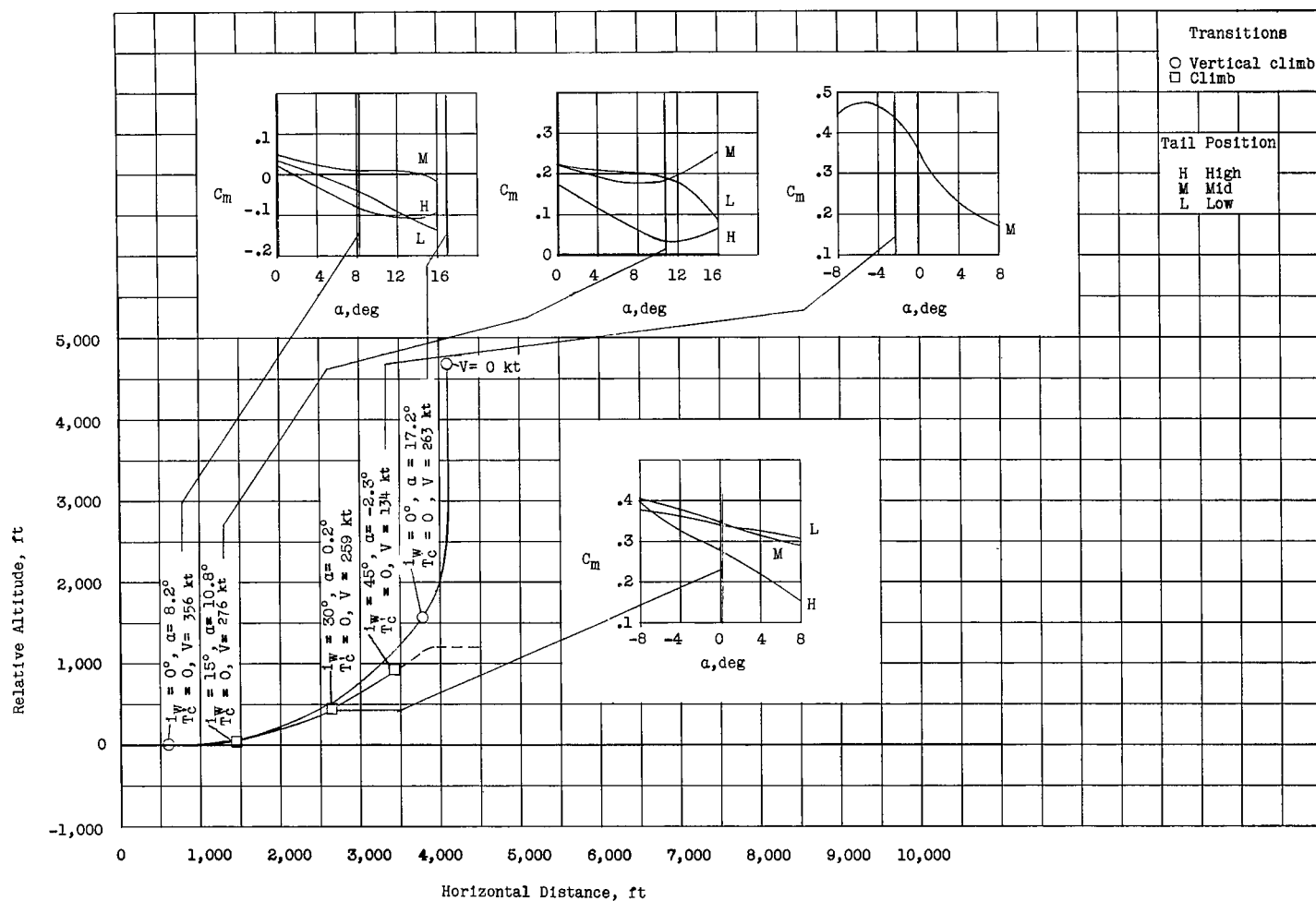
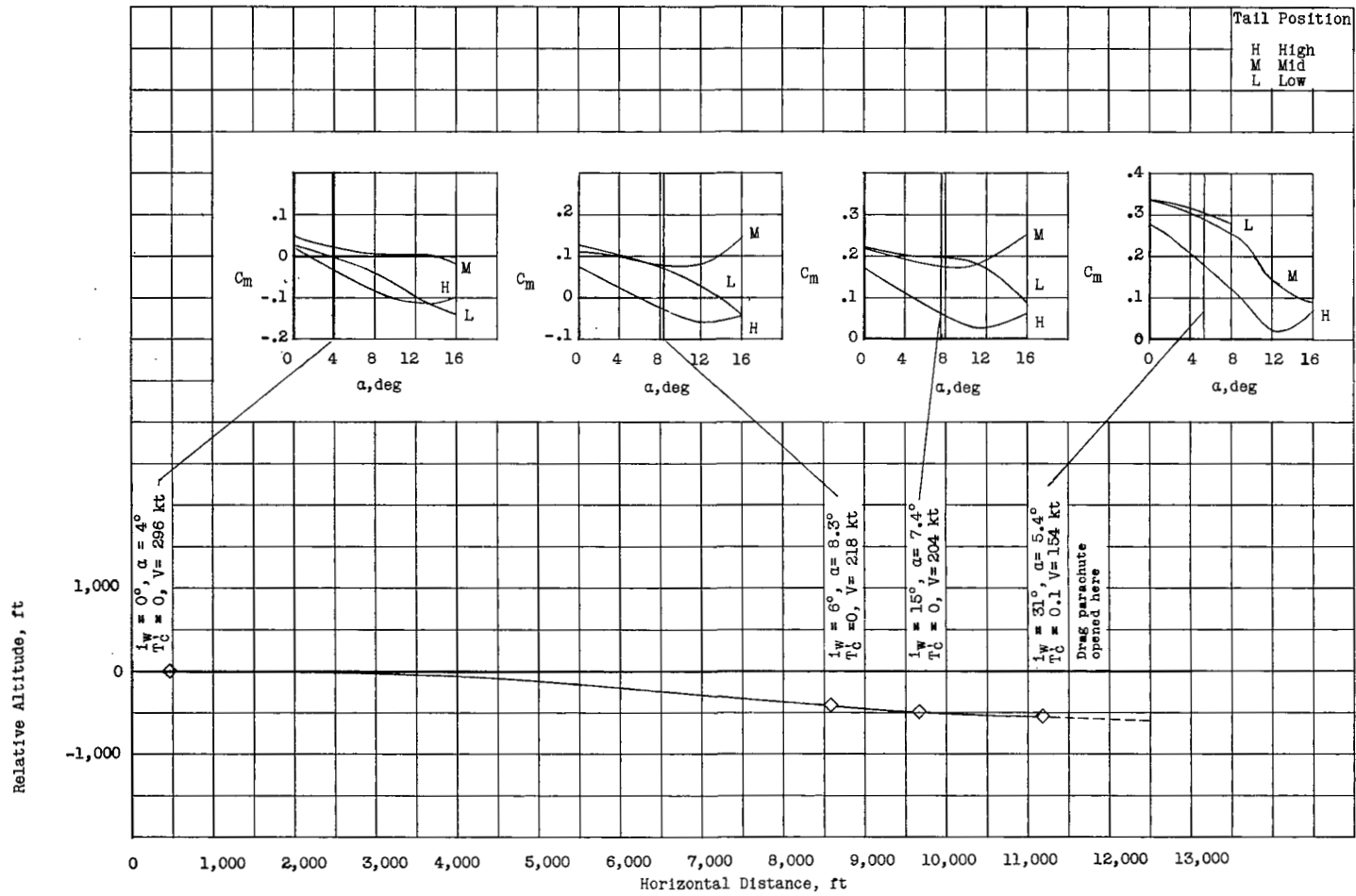


Figure 22.- Calculated take-off transition flight path for an airplane with an initial gross take-off weight of 150,000 pounds, 180,000 pounds available thrust, and 960 square feet of wing area.



(a) Vertical climb and climbing transition for landing approach.

Figure 23.- Calculated landing transition flight paths for an airplane with a gross initial landing weight of 65,000 pounds and a wing area of 960 square feet.



(b) Level transition for landing approach.

Figure 23.- Concluded.

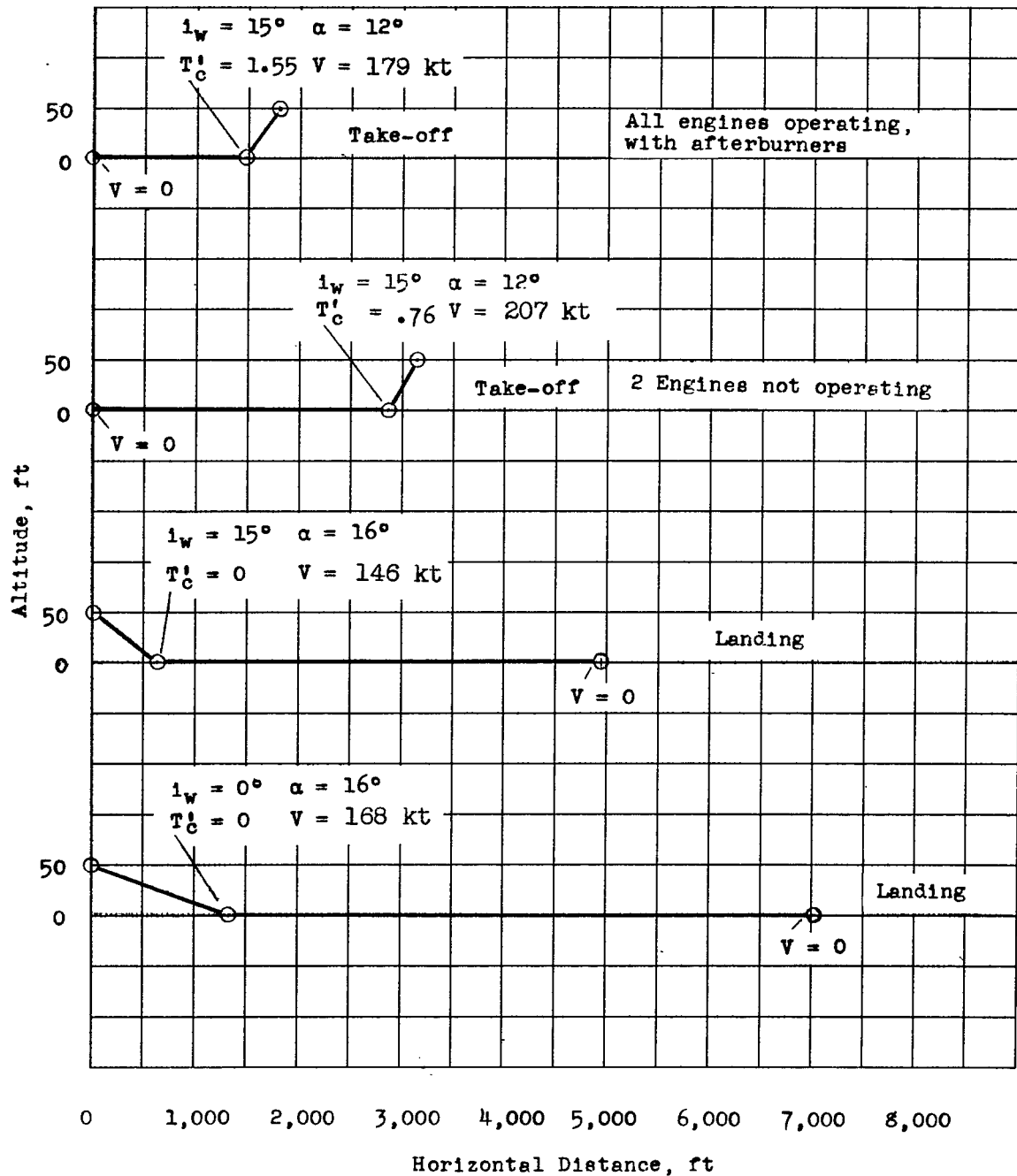


Figure 24.- Take-off and landing distances and conditions using conventional take-off and landing.

NASA Technical Library



3 1176 01438 0688

CONFIDENTIAL